

1 **Tracing marine cryptotephra in the North Atlantic during the Last Glacial Period:**
2 **Improving the North Atlantic marine tephrostratigraphic framework**

3

4 Peter M. Abbott^{1,2,3,*}, Adam J. Griggs¹, Anna J. Bourne^{1,4}, Mark R. Chapman⁵, Siwan M.
5 Davies¹

6

7 ¹Department of Geography, College of Science, Swansea University, Singleton Park,
8 Swansea, SA2 8PP, UK

9 ²School of Earth and Ocean Sciences, Cardiff University, Park Place, CF10 3AT, Cardiff, UK

10 ³Institute of Geological Sciences and Oeschger Center for Climate Change Research,
11 University of Bern, Baltzerstrasse 1+3, Bern 3012, Switzerland

12 ⁴Geography and Environment, University of Southampton, University Road, Southampton,
13 SO17 1BJ, UK

14 ⁵School of Environmental Sciences, University of East Anglia, Norwich Research Park, NR4
15 7TJ, UK

16

17 *Corresponding author (abbottp@cardiff.ac.uk)

18

19 ***Abstract***

20

21 Tephrochronology is increasingly being recognised as a key tool for the correlation of
22 disparate palaeoclimatic archives, underpinning chronological models and facilitating
23 climatically independent comparisons of climate proxies. Tephra frameworks integrating both
24 distal and proximal tephra occurrences are essential to these investigations providing key
25 details on their spatial distributions, geochemical signatures, eruptive sources as well as any
26 available chronological and/or stratigraphic information. Frameworks also help to avoid mis-
27 correlation of horizons and provide important information on volcanic history. Here we
28 present a comprehensive chronostratigraphic framework of 14 tephra horizons from North
29 Atlantic marine sequences spanning 60-25 cal ka BP. Horizons previously discovered as
30 visible or coarse-grained deposits have been combined with 11 newly recognised volcanic
31 deposits, identified through the application of cryptotephra identification and characterisation
32 methods to a wide network of marine sequences. Their isochronous integrity has been
33 assessed using their physical characteristics. All horizons originated from Iceland with the
34 vast majority having a basaltic composition sourced from the Grímsvötn, Kverkfjöll,

35 Hekla/Vatnafjöll and Katla volcanic systems. New occurrences, improved stratigraphic
36 placements and a refinement of the geochemical signature of the NAAZ II are reported and
37 the range of the FMAZ IV has been extended. In addition, several significant geochemical
38 populations that further investigations could show to be isochronous are reported. This tephra
39 framework provides the foundation for the correlation and synchronisation of these marine
40 records to the Greenland ice-cores and European terrestrial records to investigate the phasing,
41 rate, timing and mechanisms controlling the rapid climate changes that characterised the last
42 glacial period.

43

44 **Keywords:** Quaternary; palaeoceanography; tephrochronology; North Atlantic; tephra
45 framework; marine cores

46

47 *1. Introduction*

48

49 Tephrochronology, the use of volcanic ash deposits as isochronous tie-lines between
50 disparate palaeoclimatic records, is increasingly being utilised as a key geochronological tool
51 for reconstructing the timing and phasing of past climatic events (e.g. Lowe, 2011; Lowe et
52 al., 2012; Lane et al., 2013; Davies, 2015). This upsurge is directly linked to advances in
53 cryptotephra analysis, which has dramatically increased the number of potential tie-lines and
54 led to the compilation of regional tephra frameworks (e.g. Lowe et al., 2008; Tryon et al.,
55 2009; Zanchetta et al., 2011; Davies et al., 2012; Abbott and Davies, 2012; Lowe et al.,
56 2015). Tephrostratigraphical frameworks typically include a compilation of key information
57 relating to the tephra horizons within them, including their spatial extent, based on
58 preservation within palaeoclimate records, glass shard concentrations, glass shard
59 composition and eruptive source alongside chronological and stratigraphic information (e.g.
60 Lowe et al., 2008; Davies et al., 2014; Bourne et al., 2015; Matthews et al., 2015). The most
61 comprehensive frameworks include both distal and proximal tephra findings, visible and
62 cryptotephra occurrences and combine newly discovered data with previously published
63 deposits. Integrating all this information can provide valuable frameworks for the volcanic
64 history of a region and provide key reference tools for future studies. Distal archives are often
65 more complete than proximal records, which are prone to removal or burial of deposits,
66 although proximal archives can often record more information regarding eruptions, such as
67 their full geochemical evolution. In addition, developing the most comprehensive tephra
68 frameworks will help to reduce instances of mis-correlation which can occur if volcanic

69 regions produce multiple, closely-timed eruptions with similar geochemical compositions
70 (e.g. Lowe, 2011; Bourne et al., 2013).

71

72 For the North Atlantic region, various detailed frameworks spanning a range of time-intervals
73 are currently available. For example, Gudmundsdóttir et al. (2016) provides a proximal
74 framework of Icelandic eruptions during the Holocene, Blockley et al. (2014) summarises the
75 European tephra stratigraphy over the last glacial cycle and Davies et al. (2014) provides an
76 integrated framework of MIS 5 tephra in Greenland ice-cores and North Atlantic marine
77 records. The tephra framework for the Greenland ice-cores has significantly expanded in
78 recent years (e.g. Mortensen et al., 2005; Abbott and Davies, 2012; Davies et al., 2014), in
79 particular over the MIS 2-3 period (Bourne et al., 2015), highlighting the value of exploring
80 these distal archives. In comparison, however, only a limited number of tephra horizons have
81 been identified in North Atlantic marine records spanning MIS 2-3 (see Haflidason et al.,
82 2000; Wastegård et al., 2006; Section 2). This relative paucity is despite considerable
83 advances in distal tephrochronology and the high potential for a tephra framework from these
84 sequences to be used to establish correlations to the Greenland ice-cores and European
85 terrestrial records. Such correlations could help answer key questions regarding the relative
86 timing of atmospheric and oceanic changes associated with the rapid climatic events, that
87 punctuated the region during the last glacial period (e.g. NGRIP Members, 2004; Bond et al.,
88 1993; Martrat et al., 2007; Hall et al., 2011; Zumaque et al., 2012; Henry et al., 2016).

89

90 Here we present a tephra framework for North Atlantic marine records spanning MIS 2-3,
91 which is underpinned by our investigations of an extensive core network (Figure 1) using
92 recently developed cryptotephra identification methods (Abbott et al., in revision). Prior
93 studies are also reviewed (Section 2) and previously identified isochronous horizons are
94 integrated with our new cryptotephra discoveries. This integration represents the most
95 concerted attempt to improve the tephra framework for the North Atlantic, and overall a
96 framework of 14 marine tephra or cryptotephra horizons from between 60-25 cal ka BP has
97 been defined (Figure 2).

98

99 ***2. Prior North Atlantic Tephra Investigations between 25-60 ka BP***

100

101 It was highlighted earlier that tephra frameworks should integrate all isochronous tephra
102 deposits from a region, so the framework presented in this work integrates our new

103 discoveries alongside previously published data from multiple cores sites from the North
104 Atlantic (green sites on Figure 1). Within these prior tephrochronological studies of the MIS
105 2-3 period, several isochronous tephra horizons have been identified, i.e. North Atlantic Ash
106 Zone II (NAAZ II), Faroe Marine Ash Zone (FMAZ) II and FMAZ IV. Reviewing the
107 literature does, however, highlight some of the challenges associated with determining the
108 isochronous nature of deposits and the limitations of earlier studies that only focused on the
109 coarse fraction ($>150\ \mu\text{m}$) of the marine sediments. These were the major factors driving the
110 development of a procedure for isolating fine-grained cryptotephra (down to $25\ \mu\text{m}$
111 diameter) and interpreting transportation and depositional processes (e.g. Abbott et al., 2011,
112 in revision; Davies et al., 2014; Griggs et al., 2014). This is essential to determine the
113 isochronous nature of fine-grained, cryptotephra deposits for which macro-sedimentary
114 evidence cannot be utilised to determine the relative influence of primary and secondary
115 processes. These methods were utilised by Abbott et al. (2016) to identify three previously
116 undocumented MIS 2-3 volcanic events within a core retrieved from the Goban Spur (see
117 Section 4 for details) and are more widely applied in this study.

118

119 The first MIS 3 tephra deposit to be recognised in the North Atlantic was NAAZ II, initially
120 identified by Bramlette and Bradley (1941) and later described by Ruddiman and Glover
121 (1972). NAAZ II is a complex ash zone composed of the products of several Icelandic
122 eruptions (see Section 4.1.1) with rhyolitic material from one eruption (II-RHY-1) the most
123 widespread, being traced into multiple marine cores and the Greenland ice-cores (e.g.
124 Kvamme et al., 1989; Grönvold et al., 1995; Lacasse et al., 1996; Zielinski et al., 1997;
125 Haflidason et al., 2000; Austin et al., 2004; Svensson et al., 2008). The widespread nature of
126 II-RHY-1 gives rise to a key tie-line between North Atlantic marine records and the
127 Greenland ice-cores within the North Atlantic tephra framework (Austin and Abbott, 2010).

128

129 The FMAZs comprise a series of ash zones identified in cores around the Faroe Islands
130 region, and three, II, III and IV, were deposited during MIS 2-3. Two of these, FMAZ II and
131 IV, have isochronous characteristics and are integrated within the framework (Figures 1 and
132 2; Rasmussen et al., 2003; Wastegård et al., 2006; Wastegård and Rasmussen, 2014; Griggs
133 et al., 2014). FMAZ II was described by Wastegård et al. (2006) as a visible horizon and was
134 suggested to be a widespread primary fall deposit. The FMAZ II was subsequently traced into
135 the NGRIP ice-core by Davies et al. (2008) (NGRIP 1848 m; $26,740 \pm 390\ \text{yr b2k}$), providing
136 a clear demonstration of the high potential for ice-marine correlations between the Greenland

137 ice-cores and North Atlantic marine sequences during the 60-25 cal ka BP period. FMAZ IV
138 was first described by Wastegård and Rasmussen (2014) as a layer up to 20 cm thick
139 deposited shortly after warming related to Dansgaard-Oeschger (DO) event 12. Due to its
140 homogeneous composition and micro-sedimentary features (Griggs et al., 2014, 2015) it has
141 been interpreted as a primary ashfall deposit.

142

143 FMAZ III, identified as a thick relatively dispersed zone of tephra spread over ~20 cm depth
144 in the Faroes cores, was also thought to have a correlative in the NGRIP core (NGRIP
145 2066.95 m; $38,122 \pm 723$ yr b2k; Davies et al., 2010). However, Bourne et al. (2013)
146 subsequently identified a series of closely-spaced tephra horizons in the NGRIP and NEEM
147 ice-cores around NGRIP 2066.95 m, many with geochemical compositions that fall within
148 the wide geochemical envelope of FMAZ III. This highlighted the complexity of the period
149 and demonstrated that the suggested correlation was inappropriate and did not represent an
150 ice-marine tie-line (Bourne et al., 2013). Bourne et al. (2013) and Griggs et al. (2014) both
151 suggested that FMAZ III formed through the amalgamation of several separate tephra-fall
152 events and low sedimentation rates at the core sites so the diachronous deposits are not
153 incorporated in the marine tephra framework.

154

155 Early studies of North Atlantic tephra mainly focused on investigating visible tephra horizons
156 or glass shards present within the coarse fraction of the sediment (i.e. $>150 \mu\text{m}$ diameter).
157 This may have created a bias towards the identification of horizons from large scale eruptions
158 and/or horizons not deposited via primary ash-fallout (Brendryen et al., 2010; Abbott et al.,
159 2011). The study of Lackschewitz and Wallrabe-Adams (1997) highlights the limitation of
160 this approach. Several ash zones above NAAZ II were identified within and correlated
161 between a series of cores from the Reykjanes Ridge, however, most of these deposits have
162 heterogeneous geochemical compositions and in general coincide with distinct peaks in ice-
163 rafted debris (IRD). Based on these factors Lackschewitz and Wallrabe-Adams (1997)
164 concluded that this material was transported to the sites via iceberg rafting. This process
165 could have significantly delayed the deposition of these deposits and, hence, they do not
166 represent isochronous marker horizons and are not incorporated in the marine tephra
167 framework. The only deposit with isochronous characteristics was the X peak, a discrete high
168 concentration peak within VZ 1 in the SO82-5 core, with a homogeneous glass composition
169 and no coeval IRD peak. This horizon was subsequently correlated to FMAZ II by Wastegård
170 et al. (2006) (Figure 2).

171

172 Voelker and Haflidason (2015) utilised the coarse sediment fraction to define a high-
173 resolution tephrostratigraphy for the last 86 ka from the southern Greenland Sea PS2644 core.
174 This sequence was interpreted as containing a record of 68 volcanic events between ~60-25
175 cal ka BP based on the geochemical analysis of glass shards from 28 depths in the core. The
176 volcanic events, however, are sometimes defined based on a limited number of geochemical
177 analyses of deposits with multiple glass-based geochemical populations/events often
178 identified at the same depth. According to protocols for assessing deposits this heterogeneity
179 could be indicative of deposition via iceberg rafting and/or secondary depositional processes
180 (Abbott et al., in revision), however, while these processes were acknowledged a distinction
181 between tephra deposited via primary or secondary process is often not made. This may have
182 led to the overreporting of the number of isochronous deposits present so the deposits from
183 these volcanic events are not incorporated into the North Atlantic tephra framework presented
184 here. However, it is important to note these findings as a reappraisal of these deposits
185 together with IRD evidence may well reveal the presence of dominant populations and
186 valuable isochrons in the future.

187

188 **3. Methodology**

189

190 *3.1 Detecting, characterising and correlating cryptotephra deposits*

191

192 A widespread network of North Atlantic cores was investigated (Figure 1) and we applied the
193 consistent methodological approach for cryptotephra identification outlined in Abbott et al.
194 (in revision). Following preliminary low-resolution analysis, high-resolution glass shard
195 concentration profiles were gained from the core deposits. The major element composition of
196 peaks in glass shard concentrations were characterised using electron-probe micro-analysis
197 (EPMA) with at least 20-40 individual shards from each deposit analysed (see Abbott et al.,
198 in revision for full description). For all analysis and data comparison, the major element data
199 were normalised to an anhydrous basis, i.e. 100 % total oxides, however, the raw
200 geochemical data are provided in the Supplementary Data alongside secondary standard
201 analyses (Table S12). Potential sources for geochemical populations and tephra or
202 cryptotephra horizons were explored through graphical comparison of the composition of
203 individual shards with glass and whole rock analyses from proximal Holocene Icelandic
204 deposits from the three different rock suites and specific volcanic systems. We acknowledge

205 that some centres may have geochemically evolved or not been productive during the last
206 glacial period, therefore, the potential sources proposed here may need to be revised.

207

208 Potential cross-correlations between all the isochronous horizons and significant glass shard
209 derived geochemical populations in cores within the network and other marine records were
210 explored using statistical comparisons of their average geochemical signature and graphical
211 comparisons on bivariate plots. The similarity coefficient function (SC) of Borchardt et al.
212 (1972) was utilised to construct a matrix for all these comparisons (Table S13). Twenty-five
213 of the comparisons returned SC values greater than 0.97, which implies there are strong
214 similarities in the geochemical signatures and further assessment was required to determine if
215 they are correlatives. A combination of three main factors were used to rule out most of these
216 comparisons as potential correlatives: large stratigraphic discrepancies, subtle geochemical
217 differences, and occurrence at different depths in the same core sequence. Despite the
218 majority being ruled out, upon further assessment two of the comparisons with high SC
219 values were found to have very strong geochemical similarities and consistent stratigraphic
220 positions and are suggested as correlatives between marine sequences in the network (see
221 Section 4).

222

223 *3.2 Assessing the isochronous nature of cryptotephra deposits*

224

225 Several of the deposits reported here have been described in Abbott et al. (in revision) as
226 illustrative examples for assessing the dominant controls on tephra deposition in the North
227 Atlantic region. We synthesise these results in a framework of tephra deposits that represent
228 isochronous marker horizons identified using protocols set out in Griggs et al. (2014) and
229 Abbott et al. (in revision). The key characteristics used to define isochronous horizons are: (i)
230 a clear peak in the shard concentration profile that can be used as the isochron position and
231 (ii) a homogeneous geochemical population or distinct trend in glass shard analyses
232 indicative of material deriving from a single volcanic eruption. Abbott et al. (in revision)
233 outlines a tephra deposit type scheme that uses glass shard concentration profiles and
234 geochemical homogeneity/heterogeneity to identify six North Atlantic marine tephra deposits
235 types with common modes of tephra delivery and post-depositional reworking. Here that
236 scheme is utilised to aid the assessment of the deposits identified in the marine records
237 Although Type 1 and 3 deposits are typically characterised by single homogeneous
238 populations there is greater variability and complexity in the geochemical signatures of Type

239 2 deposits. For the latter a larger number, typically >30 but on occasions up to 60, of single-
240 grain major element analyses were acquired. These were graphically assessed to explore the
241 relative homogeneity or heterogeneity of deposits, define homogeneous populations that may
242 have derived from single eruptions, quantify their relative dominance within the deposits and
243 categorise them as Type 2A or Type 2B deposits. Outliers were defined as analyses that were
244 not consistently associated with a defined population. For some heterogeneous deposits
245 where populations were not identifiable analyses were grouped based on affinities to the
246 Icelandic rock suites (see Supplementary Figures).

247

248 *3.3 Age and stratigraphic constraints*

249

250 The timing of deposition for each tephra deposit is given based on the available
251 climatostratigraphy for the specific core within which the horizons were isolated (Table 1).
252 For some records, there is strong stratigraphic control based on proxy records from the cores
253 that record the DO events which characterised the North Atlantic region during the last
254 glacial period, e.g. MD04-2822 and MD04-2829CQ. However, for other cores, e.g. MD99-
255 2251 and GIK23415-9, the stratigraphic frameworks are not as distinct with deposits from the
256 Heinrich events providing the best stratigraphic control. Due to uncertainties in the relative
257 timing of closely spaced horizons not identified in the same core sequence the stratigraphic
258 relationships presented in Figure 2 should be treated with caution, e.g. the cluster of horizons
259 that have been identified in various cores around the H4 event (Figure 2). Further
260 investigations of these horizons, such as their tracing into other sequences, may help to refine
261 the sequence of the volcanic events in the future.

262

263 *4. North Atlantic Tephra Framework*

264

265 An improved marine tephra framework for the North Atlantic between 60-25 cal kyr BP is
266 presented in Figure 2 and Table 1. Overall, a framework of 14 isochronous horizons can be
267 defined, including 8 new isochronous horizons presented for the first time, 3 cryptotephra
268 deposits identified in MD04-2820CQ by Abbott et al. (2016) and 3 previously published
269 deposits (NAAZ II, FMAZ IV and FMAZ II). This new framework represents a significant
270 increase in the number of tephra marker horizons that could be utilised for the correlation of
271 records during this period.

272

273 With the exception of NAAZ II (II-RHY-1) and MD04-2820CQ 497-498 cm, all tephras in
274 the framework are basaltic in composition and originated from Iceland, specifically from the
275 Grímsvötn, Kverkfjöll, Hekla/Vatnafjöll and Katla volcanic systems (Table 1). The most
276 widespread isochronous horizon in the framework is the NAAZ II (II-RHY-1) (Figures 3 and
277 4). The wide distribution and importance of this horizon had been established in prior studies,
278 however, here we have isolated it in more sequences, gained greater control on the timing of
279 deposition, with peaks in shard concentration determined at a 1 cm resolution, and provided
280 an improved glass geochemical signature for the horizon (Section 4.1.1). The geographical
281 range of the previously identified FMAZ IV can be expanded, to a limited extent, from the
282 Faroe Islands region to the Norwegian Sea following its identification in MD95-2010 (Figure
283 5; Section 4.1.2).

284

285 Within our network only two cores, MD04-2822 and MD04-2829CQ, exclusively preserved
286 isochronous Type 1 deposits (Figures 6a and 6b). New isochronous horizons were also
287 identified in two further cores, MD99-2251 and GIK23415-9, alongside other deposits
288 without clear isochronous characteristics, i.e. Type 2B and Type 4 deposits (Figures 7a and
289 8a), which can be attributed to temporal variability in the processes controlling tephra
290 deposition at these sites (see Abbott et al., in revision). Further details regarding all the
291 isochronous horizons are provided in Section 4.1 in chronological order from the oldest to the
292 youngest horizon.

293

294 The Type 2B and Type 4 horizons are not overlooked though as analysis showed that within
295 many of these deposits significant homogeneous geochemical populations could be isolated
296 (Figures 7b and 8b; Table 1). These populations are presented alongside the framework of
297 isochronous horizons as their geochemical homogeneity suggests that they were derived from
298 single volcanic events, but, at present, questions remain over their depositional origin and
299 isochronous nature. Further investigations, however, may permit their integration into the
300 regional tephra framework and this is discussed further in Section 4.2.

301

302 *4.1 Isochronous horizons*

303

304 *4.1.1 NAAZ II*

305

306 NAAZ II is a crucial deposit within the North Atlantic marine tephra framework and it has
307 been identified at nine sites within our network as a clear peak in rhyolitic material and at 6
308 sites basaltic/intermediate material was also present. Based on occurrences of NAAZ II in
309 several North Atlantic sites, this ash zone was defined as being composed of five
310 geochemical populations, one rhyolitic (II-RHY-1) and four basaltic (II-THOL-1, II-THOL-
311 2, II-THOL-3 and II-TAB-1) by Kvamme et al. (1989).

312

313 Shards from the peaks in rhyolitic material at the 9 sites have a consistent homogeneous
314 transitional alkali rhyolitic composition (Figure 3a(i) and 4b; Table S2). In comparison to
315 prior characterisations of NAAZ II from several North Atlantic marine cores, strong
316 similarities can be observed for some oxides, e.g. FeO and CaO (Figure 3bi) but some offsets
317 are apparent for other oxides, e.g. Na₂O and SiO₂ (Figure 3bii). These differences are
318 reflected in similarity coefficient comparisons (Table S2) and are consistent with sodium loss
319 affecting the older EPMA analyses (Hunt and Hill, 1993; Kuehn et al., 2011), particularly for
320 the analyses from Kvamme et al. (1989), and are highly unlikely to indicate a different source
321 for the material. Therefore, the nine deposits in this network can be correlated to the II-RHY-
322 1 component of NAAZ II. These new analyses provide an up-to-date composition for this
323 component and highlight that data quality must be considered when assessing correlations
324 between datasets, especially for rhyolitic material.

325

326 A peak in brown shards was isolated in direct association with the II-RHY-1 peak at 6 sites
327 (Figure 4b; e.g. in MD99-2251 (Figure 4a)). Compositional analyses revealed a range of
328 signatures with basaltic and intermediate material present (Figure 3a(ii)). Shards related to
329 three of the basaltic populations of Kvamme et al. (1989) have been identified, but no shards
330 related to the II-THOL-3 population were isolated (Figure 3c). Glass shards with an
331 intermediate trachyandesite to trachydacite composition have been identified (Figure 3a(ii))
332 and grouped as a new population, which we name II-INT-1. Some material with an
333 intermediate composition was found in association with the proximal Icelandic deposit
334 correlated to NAAZ II, the Thorsmörk ignimbrite (Jørgensen, 1980). However, this is less
335 evolved than the material in these marine deposits with SiO₂ values of 56-58 % and is
336 unlikely to be directly related. This additional intermediate population suggests that the
337 basaltic material associated with NAAZ II derives from more individual eruptions than
338 previously thought. This assertion is also supported by differences in the composition of
339 material from this study attributed to the populations of Kvamme et al. (1989) which may

340 indicate they grouped material from multiple eruptions as single populations. For example,
341 shards from M23485-1 and GIK23415-9 display geochemical differences, e.g. Figure 3cii,
342 despite all falling into the II-THOL-2 field of Kvamme et al. (1989). At three of the sites the
343 brown shards can be grouped as single populations: homogeneous populations within the II-
344 THOL-2 geochemical field in M23485-1 and JM11-19PC and only shards from the
345 intermediate population are present in MD01-2461 (Figure 4c). The remaining three sites
346 preserve a mix of populations. MD04-2820CQ preserves three populations (II-THOL-1, II-
347 THOL-2 and II-INT-1), each exceeding 24% of the shards present. GIK23415-9 and MD99-
348 2251 are dominated by the II-THOL-1 and II-TAB-1 populations, respectively.

349

350 The contrast between the homogeneity of the rhyolitic material at all sites and the
351 heterogeneity and inconsistent signatures of the basaltic/intermediate material may indicate
352 that despite coeval deposition the two components were transported differentially. It has been
353 suggested that NAAZ II was primarily transported from Iceland via sea-ice rafting and
354 primary airfall (e.g. Ruddiman and Glover, 1972; Austin et al., 2004; Wastegård et al., 2006).
355 Sea-ice rafting may have contributed towards the relatively higher rhyolitic shard
356 concentrations at sites to the south and west of Iceland. The geochemical homogeneity and
357 distinct peak with an upward tail in rhyolitic shard concentrations (i.e. Type 3 deposits; e.g.
358 Figure 4a(i)), observed at all sites is consistent with these transport processes and supports
359 the isochronous nature of the II-RHY-1 component.

360

361 The heterogeneity of the basaltic material and relative discreteness of the concentration
362 peaks, e.g. Figure 4a(ii), are consistent with transport via iceberg rafting and the between-site
363 contrasts in geochemical signatures highlights that icebergs calved from different margins of
364 the Icelandic ice sheet could have transported and deposited material at the core sites. The
365 absence of basaltic material associated with the rhyolitic peaks in the MD04-2822 and
366 MD95-2010 sites is consistent with the findings of Abbott et al. (in revision) that ice rafting
367 did not transport tephra to these sites during the last glacial period. Transportation via iceberg
368 rafting can delay the deposition of tephra: therefore the peaks in basaltic material related to
369 NAAZ II should not be utilised as isochronous markers. However, based on their dominance
370 as homogeneous populations at some sites, II-THOL-2, II-TAB-1 and II-INT-1 are regarded
371 as significant geochemical populations (Table 1). It cannot be ruled out that one or more of
372 the basaltic populations were deposited coevally via primary fallout with the rhyolitic
373 material, particularly at sites only containing one population. However, it is unlikely that this

374 process deposited all of the basaltic populations with subsequent amalgamation in the
375 sediment column, as shard concentrations profiles for that type of deposit (Type 4) typically
376 have a greater vertical spread within sequences and display multiple concentration peaks.

377

378 The coeval deposition of the two shard types may indicate that the volcanic eruption that
379 produced the rhyolitic tephra horizon triggered an ice-rafting event which deposited the
380 basaltic material, but the resolution of the marine records under investigation here is
381 insufficient to resolve this temporal phasing.

382

383 *4.1.2 FMAZ IV – MD95-2010 915-916 cm*

384

385 FMAZ IV was identified in the MD95-2010 core from the Norwegian Sea as a discrete
386 deposit at 915-916 cm depth (Figure 5a). This deposit has a homogeneous basaltic glass
387 composition with affinities to the Icelandic tholeiitic rock suite and the products of the
388 Grímsvötn volcanic system. The glass composition of MD95-2010 915-916 cm is identical to
389 the characterisation of the JM11-19PC 542-543 cm deposit of Griggs et al. (2014) (Figure 5b;
390 SC – 0.985), previously correlated to the FMAZ IV of Wastegård and Rasmussen (2014).
391 According to the age model and stratigraphy for MD95-2010 from Dokken and Jansen
392 (1999), this layer has an age of ~44.45 cal ka BP and was deposited during the DO-12 event
393 based on the magnetic susceptibility record. This stratigraphic position and age estimate are
394 consistent with the work of Wastegård and Rasmussen (2014). This horizon has previously
395 not been identified outside the Faroe Islands region and, therefore, this discovery expands its
396 geographical range in a northeasterly direction to the Nordic Sea.

397

398 *4.1.3 MD04-2820CQ 524-525 cm*

399

400 MD04-2820CQ 524-525 cm has previously been described by Abbott et al. (2016) where it
401 was identified as a clear peak in shard concentrations spanning ~6 cm depth. Geochemical
402 analyses of shards from this deposit form a homogeneous tholeiitic basaltic population
403 sourced from either the Grímsvötn or Kverkfjöll Icelandic volcanic systems. These
404 characteristics allow the deposit to be defined as Type 2A and, allied with a lack of direct
405 covariance with IRD, this deposit is thought to have been deposited via primary fallout
406 despite occurring during a period of elevated IRD concentrations (Abbott et al., 2016).

407

408 *4.1.4 MD04-2822 2017-2018 cm*

409

410 High-resolution analysis of MD04-2822 showed a well-constrained peak in brown glass
411 shards in all grain-size fractions at 2017-2018 cm depth (Figure 6a). According to the core
412 stratigraphy, this horizon was deposited during a stadial period prior to the warming
413 transition into DO-9 (Figure 6a). Shards have a homogeneous basaltic composition with
414 affinities to the Icelandic tholeiitic rock suite and the products of the Grímsvötn volcanic
415 system (Figure 6c).

416

417 *4.1.5 MD04-2820CQ 497-498 cm*

418

419 MD04-2820CQ 497-498 cm was identified as a small peak in colourless glass shards, during
420 a period of consistently elevated shard concentrations, deposited prior to DO-9 (Abbott et al.,
421 2016). Shards from the peak have a transitional alkali rhyolitic composition and form a single
422 population with affinities to a number of distal tephra deposits previously attributed to the
423 Katla volcanic system (Abbott et al., 2016). This horizon is notable as it is the only other
424 rhyolitic horizon within the marine tephra framework apart from the rhyolitic component of
425 NAAZ II (Table 1). Due to its homogeneity and the prevalence of shards in the 25-80 μm
426 fraction, this deposit was interpreted as an isochronous horizon deposited via primary ashfall
427 (Abbott et al., 2016).

428

429 *4.1.6 MD04-2820CQ 487-488 cm*

430

431 Deposited just prior to Heinrich Event 4, MD04-2820CQ 487-488 cm was identified as a
432 clear peak in brown glass shard concentrations across all grain size fractions spread over ~3
433 cm depth (Abbott et al., 2016). While some transitional alkali outliers are present within
434 shard analyses from this deposit, the vast majority of shards (~85 %) form a homogeneous
435 geochemical population with a tholeiitic basaltic composition and affinities to the Grímsvötn
436 volcanic system (Abbott et al., 2016). This homogeneous composition and a lack of
437 covariance of shard concentrations with IRD suggests it was not deposited via iceberg rafting.
438 Deposition is likely to have occurred via primary fall, however, the high proportion of shards
439 in the coarser grain-size fractions (80-125 μm and >125 μm) in comparison to the 25-80 μm
440 fraction may also indicate transport via sea-ice rafting. Neither transport process would

441 impart a significant temporal delay in deposition, therefore, MD04-2820CQ 487-488 cm is
442 viewed as an isochronous deposit (Abbott et al., 2016).

443

444 *4.1.7 MD04-2829CQ 934-935 cm and 930-931 cm*

445

446 Two distinct and closely spaced peaks in brown glass shards were isolated in MD04-2829CQ
447 with concentrations of ~35 shards per 0.5 g dws in the 25-80 μm grain-size fraction (Figure
448 6b). Only a limited number of shards were isolated in one of the three samples between these
449 peaks. The stratigraphy for MD04-2829CQ indicates that these horizons were deposited
450 during and just after the rapid warming into DO-8 (Figure 6b; Hall et al., 2011). Shards from
451 both peaks were geochemically analysed and the analyses revealed two homogeneous
452 basaltic populations with affinities to the Icelandic tholeiitic rock suite and the products of the
453 Grímsvötn volcanic system. However, there are distinct differences in Al_2O_3 , FeO, CaO and
454 MgO between the two deposits (Figure 6c). These differences show that despite being
455 separated by only 3 cm of sediment the horizons were produced by two separate volcanic
456 eruptions and, coupled with their other characteristics, can both be considered as valuable
457 isochronous marker horizons.

458

459 *4.1.8 MD04-2822 2004-2005 cm*

460

461 High-resolution shard counts identified brown shards within the 25-80 and >125 μm grain-
462 size fractions in the 2004-2005 cm sample of MD04-2822 (Figure 6a). While the shard
463 concentrations are low the peaks are discrete as no further shards were identified in adjacent
464 samples. Based on the stratigraphy of the core this material was deposited shortly after the
465 warming transition into DO-8 (Figure 6a; Hibbert et al., 2010). Geochemical analysis shows
466 that shards from the deposit have a homogeneous transitional alkali basaltic composition
467 (Figure 6c). The shards are characterised by high TiO_2 values of ~4.65 %wt and comparisons
468 to proximal Icelandic deposits demonstrate that the deposit was most likely sourced from the
469 Katla volcanic system (Figure 6c). The geochemical composition of the material in this peak
470 is markedly distinct from the material in the underlying MD04-2822 2017-2018 cm horizon,
471 indicating that they represent two discrete eruption events.

472

473 *4.1.9 MD99-2251 1680-1681 cm*

474

475 The highest brown shard concentrations in MD99-2251 were identified as a peak centred
476 around 1680-1681 cm depth (Figure 7a). Overall, high shard concentrations associated with
477 this peak cover approximately 10 cm depth, typical of a Type 2 deposit, and glass shards
478 from the main peak and a secondary peak at 1683-1684 cm were geochemically analysed.

479

480 Shards from 1680-1681 cm form a clear near-homogeneous population, with 76 % of the
481 analyses in this population (Figure 7b). High TiO₂ concentrations in excess of 4.4 %wt
482 strongly indicate an origin from the Katla volcanic system (Figure 7b). Within the remaining
483 25 % of shards a minor population (6 %) of tholeiitic material, most likely sourced from the
484 Kverkfjöll volcanic system, was also identified alongside several outlying shards (Figure 7b).
485 The significant dominance of a single homogeneous population in the 1680-1681 cm peak,
486 suggests that this material was deposited via primary ashfall and that this tephra deposit
487 represents an isochronous marker horizon despite being deposited during a period of elevated
488 IRD concentrations associated with Heinrich Event 3 (Figure 7a).

489

490 The glass-derived geochemical signature of material from the underlying 1683-1684 cm peak
491 is the same as that of the major 1680-1681 cm peak suggesting that this does not represent an
492 earlier and separate depositional event but instead represents downward reworking of
493 material from the main concentration of glass. The slight deviation of the shard concentration
494 profile from a gradational downward tail could imply that any reworking processes were not
495 uniform across the core. Such variability was observed by Griggs et al. (2015) in 3D
496 reconstructions of the structure of tephra deposits gained using X-ray microtomography.

497

498 *4.1.10 MD04-2829CQ 800-801 cm*

499

500 The highest shard concentrations in core MD04-2829CQ were identified at 800-801 cm, with
501 increases observed in all grain-size fractions (Figure 6b). This deposit is very discrete with
502 limited shards identified in adjacent samples. Stratigraphic constraints indicate that this
503 horizon was deposited in the cold period prior to DO-4 (Figure 6b; Hall et al., 2011).

504 Compositional analysis of individual shards shows that all material has a tholeiitic basaltic
505 composition and can be grouped into two homogeneous populations, with clear bimodality
506 observed for some oxides, including TiO₂, FeO, CaO and MgO (Figure 6c). Analyses
507 grouped into population THOL-1 were only derived from shards from the 25-80 µm grain-
508 size fraction, whereas the majority of analyses in population THOL-2 are from shards >80

509 μm in diameter. Based on comparisons to proximal Icelandic deposits, THOL-1 has a close
510 affinity to products of Grímsvötn while THOL-2 is most likely derived from the Kverkfjöll
511 volcanic system (Figure 6b; e.g. Óladóttir et al., 2011). This implies that the deposit was
512 formed from the deposition of material from two coeval eruptions of these volcanic centres.

513

514 *4.1.11 MD04-2822 1836-1837 cm - GIK23415-9 225-226 cm*

515

516 Within the MD04-2822 record the largest peak in brown shards was identified at 1836-1837
517 cm depth with >40 shards per 0.5 g of dws present in the 25-80 μm fraction (Figure 6a). The
518 material is stratigraphically well constrained with only 2 shards present in the underlying
519 sample. According to the stratigraphy this material was deposited during the cold stadial
520 period shortly before the transition into DO-4 (Hibbert et al., 2010). Compositional analysis
521 of glass shows that material from this peak has a transitional alkali basaltic composition and
522 forms a homogeneous geochemical population (Figure 6c). Comparisons to proximal
523 Icelandic deposits indicate that the horizon was sourced from either the Katla or
524 Hekla/Vatnafjöll volcanic system (Figure 6c).

525

526 A discrete peak in shard concentrations, restricted to 1 cm and with the characteristics of a
527 Type 1 deposit, was also isolated between 225-226 cm in GIK23415-9 (Figure 8a).
528 Geochemical analysis of the shards from this deposit shows that all have a transitional alkali
529 composition (Figure 8b). Within the analyses bimodality can be observed for some oxides,
530 most notably TiO_2 , and they can be split into two homogeneous populations. A dominant
531 population (TAB-1) of 70 % of the shards with low TiO_2 values and a smaller population
532 (TAB-2) of 15 % of the analysed shards with TiO_2 values $\sim 0.35\%$ wt higher. TiO_2 values
533 have been identified as one of the primary oxides that can be used to discriminate between
534 Icelandic basaltic eruptions from the last glacial period (e.g. Bourne et al., 2013, 2015). The
535 remaining 15 % of analyses are classified as outliers. Comparisons to proximal deposits show
536 that the populations have similarities to the products of both the Katla and Hekla/Vatnafjöll
537 volcanic systems (Figure 8b). GIK23415-9 225-226 cm was deposited during Heinrich Event
538 3 which could suggest it was deposited via iceberg rafting. However, the relative dominance
539 of the TAB-1 population and a lack of direct covariance of shard concentrations with IRD,
540 with the discrete shard peak contrasting with elevated IRD concentrations for ~ 25 cm of core
541 depth, do not support this interpretation. These indicators provide support for primary ashfall

542 deposition of glass shards from either a single chemically bimodal eruption or two eruption
543 events very close in time.

544

545 Statistical analysis (SC of 0.987) and graphical comparisons support a correlation between
546 MD04-2822 1836-1837 cm and GIK23415-9 225-226 cm (TAB-1) (Table S13; Figure 9a). In
547 addition, there is a consistency in the stratigraphic position of the two horizons. MD04-2822
548 1836-1837 cm was deposited between DO events 5 and 4 (Figure 6a), while GIK23415-9
549 225-226 cm was deposited at the end of Heinrich Event 3 (Figure 8a), which, based on a
550 comparison of ages for the Heinrich Events from Sanchez Goñi and Harrison (2010) and the
551 Greenland ice-core chronology presented in Seierstad et al. (2014), occurred after Greenland
552 Interstadial (GI) 5, the ice counterpart to DO-5. Based on the available information, we assert
553 that these two deposits are the products of the same volcanic event and form a tie-line
554 between the two relatively closely spaced sequences (Figure 2).

555

556 *4.1.12 GIK23415-9 173-174 cm*

557

558 A peak in basaltic glass shard concentrations was identified in the GIK23415-9 core at a
559 depth of 173-174 cm, following Heinrich Event 2 (Figure 8a). The shard concentration
560 profile of this deposit is akin to a Type 1 deposit with a relatively discrete peak in shard
561 concentrations restricted to ~1 cm (Figure 8a). Geochemical analysis of shards from this
562 deposit show one clear homogeneous population, composed of 60 % of the analysed shards,
563 with a basaltic tholeiitic composition and an affinity to the Kverkfjöll volcanic system
564 (Figure 8b). The remaining 40 % are heterogeneous and can be regarded as outliers (Figure
565 S8). Although the overall homogeneity of the deposit is not as distinct as most Type 1
566 deposits, the occurrence of a homogeneous population deposited during a period of low IRD
567 input does suggest that primary fall occurred to form an isochronous deposit. The outlying
568 shards may derive from a low background of IRD input of ice-rafted shards during this
569 period. In addition, the use of the percentage abundance of populations to assess this deposit
570 has some limitations as only a low number of analyses, 15, were gained from shards within
571 this deposit.

572

573 *4.2 Significant geochemical populations and possible isochrons*

574

575 In addition to the isochronous deposits outlined in Section 4.1, six tephra deposits in the
576 MD99-2251 core and four in the GIK23415-9 sequence were assessed as having non-
577 isochronous characteristics and have been classified as Type 2B or Type 4 deposits (Figures
578 7a and 8a). The main criterion underpinning this assessment was the geochemical
579 heterogeneity of the deposits, indicative of the amalgamation of material from a number of
580 volcanic eruptions. However, while only three deposits, MD99-2251 1654-1655 cm and
581 1796-1797 cm and GIK23415-9 193-194 cm, have fully heterogeneous compositions the
582 other deposits contain 16 significant homogeneous geochemical populations, in total, within
583 their overall heterogeneity (Figure 2; Table 1). The significant geochemical populations may
584 relate to single volcanic eruptions, but due to their occurrence within heterogeneous deposits
585 further investigations are required to determine if they were deposited isochronously or
586 otherwise. The full glass-based geochemical signatures of all MD99-2251 and GIK23415-9
587 deposits and the populations identified within them are summarised in Figures S1-S14 and
588 Tables S8 and S10.

589

590 The 16 populations all have a basaltic composition and were sourced from Iceland. In
591 addition to the volcanoes which deposited isochronous horizons in the North Atlantic region,
592 i.e. Grímsvötn, Kverkfjöll, Hekla/Vatnafjöll and Katla, homogeneous glass shard populations
593 with geochemical similarities to the products of the Veidivötn-Bardarbunga and
594 Vestmannaeyjar volcanic systems were identified (Table 1; Figures 7a and 7b). Their relative
595 dominance within the deposits is variable, ranging from ~10 to 60 % of the total single-shard
596 analyses used to characterise the deposits (Tables S8 and S10).

597

598 Co-variance of shard concentration profiles with IRD records was another variable used to
599 assess the isochronous nature of the deposits (Abbott et al., in revision). Some of the deposits
600 with heterogeneous signatures were deposited during periods of elevated or rising IRD
601 concentration, which could indicate transport via iceberg rafting and a significant temporal
602 delay between eruption and deposition. However, iceberg rafting is not the only process that
603 can amalgamate the products of multiple eruptions. For example, for some deposits post-
604 depositional mixing in the sediment column of the products of several closely-timed
605 eruptions cannot be ruled out as some were isolated within periods of limited IRD deposition.
606 In this later scenario, deposition would have been via primary ashfall with no temporal delay,
607 however, determining the isochron position is challenging as complexity is often observed in
608 the shard concentration profiles. Primary fallout could also have occurred during a period of

609 ice-rafting deposition resulting in the incorporation of a homogeneous ashfall population
610 within a heterogeneous background rafted signal.

611

612 These differing scenarios and the uncertainty in the depositional processes implies that
613 further investigations are required to assess whether these populations are isochronous.
614 Consequentially we have reported the significant geochemical populations, but we have not
615 incorporated them within the regional tephra framework until further evidence is gained.
616 Such evidence may include their identification in other North Atlantic marine cores and/or
617 the Greenland ice-core tephra framework in a similar stratigraphic position. In addition, for
618 some records the covariance with IRD could not be fully explored because of the lower
619 resolution in this dataset relative to the shard concentration profiles. Improved high-
620 resolution IRD records would be highly advantageous for further assessing depositional
621 processes. An example of how tracing these populations into other records could provide
622 further insights into their isochronous nature is provided within our work.

623

624 The assessment of potential correlations (Table S13) highlighted a strong similarity between
625 the glass-based geochemical signature of FMAZ II and the THOL-1 population in the
626 GIK23415-9 202-203 cm deposit (Figure 7; Table 1). The SC comparison returned a high
627 coefficient of 0.990, demonstrating that the signatures were nearly identical, and this
628 observation is corroborated by graphical comparisons (Figure 9b). Stratigraphically, FMAZ II
629 has been identified between Heinrich Events 3 and 2 in marine records and was deposited
630 prior to an increase in IRD concentrations in the ENAM93-21 core (Rasmussen et al., 2003)
631 and after GI-3 in the Greenland ice-core stratigraphy (Davies et al., 2010). GIK23415-9 202-
632 203 cm was deposited during a period of increasing IRD concentrations related to the start of
633 Heinrich Event 2 (Figure 8a). These stratigraphic juxtapositions are consistent and, coupled
634 with the strong geochemical similarities, could imply isochronous deposition from the same
635 volcanic event. GIK23415-9 202-203 cm (THOL-1) is one of 4 homogeneous geochemical
636 populations within the deposit and, due to their co-occurrence, it was interpreted as being
637 deposited by iceberg rafting. The proposed correlation does not contradict this interpretation
638 but could demonstrate that GIK23415-9 202-203 cm (THOL-1) was deposited via primary
639 ashfall during a period when tephra from other events was rafted by icebergs. Overall, this
640 potential correlation highlights the complexity of some deposits, but demonstrates how these
641 significant glass geochemical populations are important to consider as potential isochronous
642 markers.

643

644 **5. Discussion**

645

646 *5.1 Future application of the North Atlantic marine tephra framework*

647

648 The North Atlantic marine tephra framework between MIS 2-3 has been significantly
649 improved through the most extensive application of cryptotephra methods, comprehensive
650 compositional analysis and rigorous and defined protocols to assess the isochronous nature of
651 each deposit. For a long period only a limited number of horizons had been identified in this
652 time period (Haflidason et al., 2000; Wastegård et al., 2006). Now this framework includes
653 14 isochronous horizons that have considerable promise for correlating and synchronising
654 palaeoclimatic records. There is also potential to add further isochronous markers given the
655 significant geochemical populations identified in heterogeneous deposits also reported in this
656 study.

657

658 NAAZ II remains a dominant tephra within this framework and our work has identified it in
659 numerous additional cores with greater control on the timing of deposition derived from high-
660 resolution shard counts and an improved geochemical signature for glass shards associated
661 with the widespread rhyolitic component (II-RHY-1). This tephra, with an age of $55,380 \pm$
662 1184 yr b2k in the Greenland ice-core records (Svensson et al., 2008), represents a key
663 marker horizon for the period providing an isochronous tie-line linking numerous widespread
664 marine cores and the Greenland ice-core records beyond the radiocarbon window. The
665 distribution of the FMAZ IV has been extended from the Faroe Islands region into the Nordic
666 Seas and has the potential to be a key tie-line for DO 12. However, despite being found
667 previously in several North Atlantic cores and the NGRIP ice-core (see summary map in
668 Davies et al., 2012), the FMAZ II was only found in one additional core, GIK23415-9.
669 Furthermore, most of the new cryptotephtras are single-core occurrences, highlighting
670 challenges with cryptotephra tracing within the North Atlantic Ocean. The limited tracing of
671 horizons may reflect the difficulties of detecting and isolating deposits that often only contain
672 a low concentration of shards, but could also indicate the relatively constrained dispersal of
673 the basaltic eruptions depositing material over the North Atlantic. Only one correlation has
674 been made between newly identified isochronous horizons in the framework, MD04-2822
675 1836-1837 cm and GIK23415-9 225-226 cm (Section 4.1.11; Figure 2). These cores are
676 relatively closely spaced, supporting the suggestion of limited basaltic ash dispersal.

677

678 Assessing potential correlations between the records highlighted that while a range of factors
679 demonstrated that there are few direct correlations, many of the horizons have similar major
680 element geochemical signatures, especially eruptives from the Grímsvötn and Katla volcanic
681 systems (Table 1). This conclusion corroborates the findings of Bourne et al. (2015) who
682 observed similar repetition of major element glass geochemical signatures from these systems
683 in tephra horizons in the Greenland ice-cores. This repetition is particularly notable for the
684 period around H4 as a cluster of six closely spaced horizons has been identified in the marine
685 cores (Figure 2). Of these, five horizons have similar tholeiitic glass major element basaltic
686 compositions and are thought to be derived from the Grímsvötn volcanic system. However,
687 subtle differences in geochemical signatures show they represent individual events, which
688 may be further emphasised through trace element analysis (Lowe et al., 2017).

689

690 The observations that the new cryptotephra in the North Atlantic region may have limited
691 dispersal and geochemical similarities do provide challenges for future correlation. There is,
692 however, the potential to constraint a number of rapid climate events, such as H4 and DO 8
693 and H3 as clusters of isochronous horizons are present around those events. Further
694 investigations should initially focus on sites close to those preserving the isochronous
695 horizons in this framework and/or re-evaluate previously explored sites (e.g. green sites on
696 Figure 1), with adaptations to the methodological approach discussed in Section 5.3. It is
697 imperative that potential correlations are rigorously assessed as correlating horizons or
698 populations with close, but not identical, major element glass geochemical signatures, could
699 lead to the establishment of incorrect tie-lines between records. Trace element analysis of the
700 glass shards may aid this assessment as the additional signature may show greater differences
701 between tephras (Lowe et al., 2017). Other supporting evidence such as broad stratigraphic
702 constraints and independent age estimates can also be used to support and test correlations. A
703 detailed assessment of possible correlations to the Greenland ice-cores will be discussed in a
704 forthcoming publication whereby trace element signatures are also employed to assess and
705 support correlations.

706

707 *5.2 Reconstructing Icelandic volcanic history*

708

709 This framework adds to our understanding of the volcanic history of Iceland during the last
710 glacial period between 60-25 cal kyr BP. The dominance of basaltic over rhyolitic horizons

711 and the high productivity of the Grímsvötn/Kverkfjöll and Katla volcanic systems around
712 Heinrich Event 4 and Heinrich Event 3, respectively, is consistent with the Greenland ice-core
713 tephra framework for the same period (Bourne et al., 2015). The dominance of basaltic
714 horizons in both sets of archives strongly suggests that differential dispersal of the products
715 of rhyolitic eruptions was not occurring and their paucity reflects a relatively lower frequency
716 of Icelandic rhyolitic eruptions during this period. Basaltic horizons potentially sourced from
717 other volcanic centres were observed, including the Veidivötn-Bardabunga and
718 Vestmannaeyjar volcanic systems. There are very few or no tephras in the Greenland
719 framework with glass-based geochemical similarities to those horizons, potentially due to a
720 bias in dispersal direction, a low number of eruptions from these sources and/or the nature of
721 volcanic eruptions from these systems. This observation shows that a more complete
722 reconstruction of Icelandic volcanism will be gained by integrating the two frameworks.
723 There is, however, a notable difference between the number of tephra deposits identified
724 between the marine and ice-core records. With 99 volcanic events recorded in the Greenland
725 records in contrast to 33 events in the marine archives, if the homogeneous populations are
726 assumed to derive from individual volcanic events. The lower resolution of the marine
727 records, the potential for the amalgamation of airfall deposits, post-depositional reworking
728 processes and the masking of low concentration glass shard deposits (see below) are the most
729 likely causes of this disparity.

730

731 *5.3 Improving the marine tephra framework*

732

733 This work has demonstrated the potential of identifying isochronous cryptotephras in North
734 Atlantic marine records of the last glacial period. However, the methodology employed to
735 identify cryptotephras in this work most likely created a bias towards the identification of
736 horizons depositing a high concentration of glass shards at core sites. As discussed by Timms
737 et al. (2017), the process of completing low-resolution scans prior to a subjective peak
738 selection for high-resolution (1 cm) analysis may introduce a bias as low concentration or
739 discrete peaks might not have sufficient shard concentrations to be observed in the low-
740 resolution record. The background of shards that is prevalent at some marine sites could mask
741 individual eruptions that deposited a low concentration of shards. In the ice-core records,
742 tephra events have been defined on the basis of as few as 3 shards (Bourne et al., 2015).
743 Detecting deposits of this kind would be particularly challenging in the marine environment
744 as they could be dismissed as “background” concentrations or hidden with the upward or

745 downward tail of a deposit or within an ash-rich deposit. We have attempted to explore the
746 presence of such horizons in this study but agree with Timms et al. (2017) who advocate the
747 use of more high-resolution shard concentration and glass-based chemical analyses to
748 improve tephrostratigraphies, while acknowledging that this may be limited by sediment
749 availability, time and financial considerations.

750

751 The marine tephra framework presented in this study should not be viewed as complete.
752 However, by focusing on maximising the number and geographical range of sequences an
753 initial framework has been produced that is a significant step towards a more comprehensive
754 tephra-based synchronisation of North Atlantic marine records. Coupling the success of the
755 methodology, the initial framework presented here and the insights into the spatial controls
756 on tephra deposition discussed in Abbott et al. (in revision), there is huge potential to add to
757 and refine the marine tephra framework. This can be achieved through focusing on new cores
758 from areas with a high potential to preserve isochronous horizons and reassessing previously
759 investigated cores at a high-resolution over key intervals during which isochronous horizons
760 were identified in this work. In addition, innovative techniques for the identification and
761 quantification of tephra that are currently being developed, for example X-ray fluorescence
762 core scanning (e.g. Kolling and Bauch, 2017), hyperspectral core imaging (e.g. Aymerich et
763 al., 2016) and automated flow cytometry and microscopy (e.g. D'Anjou et al., 2014), could
764 be tested and incorporated into the methodological approach if appropriate.

765

766 **6. Conclusions**

767

768 A consistent methodology for the identification and characterisation of marine cryptotephra
769 and the rigorous assessment of the influence of transportation and deposition processes on
770 tephra deposits were used to build an enhanced North Atlantic marine tephra framework.
771 Eleven isochronous deposits were identified in a wide network of marine sequences and have
772 been integrated with prior data to create a marine tephra framework for the MIS 2-3 period.
773 Key information for each deposit, such as their spatial extent, geochemical signature, eruptive
774 source and timing of deposition, is synthesised. A number of significant geochemical
775 populations are also reported that require further work to assess whether they originate from
776 single volcanic eruptions and were deposited isochronously via primary tephra fallout.

777

778 There is considerable potential to improve this framework by tracing the deposits into other
779 marine sequences, by identifying new deposits and/or gaining trace element characterisations
780 to aid the differentiation of closely-spaced horizons. Combining this framework with
781 knowledge of the processes controlling the deposition of tephra in the North Atlantic and the
782 identification of key areas where isochronous horizons are preserved provided in Abbott et al.
783 (in revision) these future investigations could be highly focussed, both temporally and
784 spatially. The full potential of this framework will only be realised if attempts are made to
785 trace these horizons into other archives such as the Greenland ice-cores and terrestrial
786 records. If successful they can act as time-synchronous tie-lines to correlate and synchronise
787 these palaeoclimatic records, providing insights into the phasing, rate, timing and
788 mechanisms forcing the rapid climate changes that characterised this period.

789

790 **Acknowledgements**

791

792 This work was financially supported by the European Research Council (TRACE project)
793 under the European Union's Seventh Framework Programme (FP7/2007-2013)/ERC grant
794 agreement no. [259253]. PMA also acknowledges support from the European Research
795 Council under the European Union's Horizon 2020 research and innovation programme
796 (grant agreement No 656381). We also acknowledge funding by NERC (NE/F020600/1,
797 NE/F02116X/1, NE/F021445/1) for the SMART project which contributed towards the
798 research ideas presented in this work. Thanks are due to William Austin, Henning Bauch,
799 Frederique Eynaud, Ian Hall, Claude Hillaire-Marcel, Elisabeth Michel, Tine Rasmussen,
800 Bjørg Risebrobakken, James Scourse, Mara Weinelt and the British Ocean Sediment Core
801 Research Facility (BOSCORF) for providing samples or access to the marine cores utilised
802 within this study. We would like to thank Dr Chris Hayward for his assistance with the use of
803 the electron microprobe at the Tephrochronology Analytical Unit, University of Edinburgh.
804 Gareth James, Gwydion Jones and Kathryn Lacey (Swansea University) are thanked for
805 assistance with laboratory processing. Thanks to David Lowe and Stefan Wastegård for their
806 comprehensive reviews that have helped to improve this manuscript. This paper contributes
807 to the EXTRAS project (EXTending TephRAS as a global geoscientific research tool
808 stratigraphically, spatially, analytically, and temporally within the Quaternary), an INTAV-
809 led project (International Focus Group on Tephrochronology and Volcanism) within the
810 Stratigraphy and Chronology Commission (SACCOM) of the International Union for
811 Quaternary research (INQUA).

812

813

814 **Figures**

815

816 **Figure 1:** Location map of cores within the marine network (red) and other cores referred to
817 in the text (green). Location (1) includes cores SO82-2, SO82-5, LO09-23, LO09-21, SO82-7
818 and SO82-4 described in Lackschewitz and Wallrabe-Adams (1997). Location (2) includes
819 cores ENAM93-21 and ENAM93-20 and location (3) includes cores LINK16, LINK17,
820 LINK15 and LINK04 described in Rasmussen et al. (2003), Wastegård et al. (2006) and
821 Wastegård and Rasmussen (2014).

822

823 **Figure 2:** Schematic representation of the improved marine tephra framework for the North
824 Atlantic between 60-25 cal kyr BP. Ages and the stratigraphic relationship of tephra horizons
825 between cores are approximate should be treated with caution, see text for details. The ages
826 utilised are based on either existing age models for sequences or estimates based on
827 stratigraphic positions. Heinrich Events 2-5 are included as stratigraphic markers and their
828 ages are based on those given in Sanchez Goñi and Harrison (2010).

829

830 **Figure 3:** (a) Total alkali v silica plot focusing on (i) rhyolitic material and (ii) basaltic and
831 intermediate composition glass material from NAAZ II deposits in the marine network. (b)
832 Comparison of new characterisations of NAAZ II rhyolitic glass to characterisations from
833 prior studies. Geochemical fields based on analyses of glass from deposits in cores V23-23,
834 V27-114, V23-82, V23-81 and V23-42 (Kvamme et al., 1989), MD95-2006 (Austin et al.,
835 2004), ENAM93-20, ENAM33 and EW9302-2JPC (Wastegård et al., 2006) and MD99-2289
836 (Brendryen et al., 2011). (c) Comparison of basaltic glass from newly characterised NAAZ II
837 deposits to basaltic NAAZ II glass-based populations defined by Kvamme et al. (1989). All
838 geochemical data plotted on a normalised anhydrous basis.

839

840 **Figure 4:** (a) Tephrostratigraphy of MD99-2251 between 1950-2030 cm covering the depth
841 interval of NAAZ II. (i) Rhyolitic glass shards in the 25-80 μm grain-size fraction. (ii)
842 Basaltic glass shards in the 25-80 μm grain-size fraction. (b) Peak concentrations of
843 colourless (rhyolitic) and brown (basaltic) glass shards in tephra and cryptotephra deposits
844 related to North Atlantic Ash Zone II. (c) Relative proportion of geochemical populations
845 within analyses of basaltic glass tephra shards from NAAZ II deposits at six sites within the
846 marine core network. Shard analyses not linked to the previously published populations or II-
847 INT-1 were classified as uncorrelated.

848

849 **Figure 5:** (a) High-resolution concentration profiles of brown glass shards between 910-920
850 cm in MD95-2010. (b) Comparison of the glass shard composition of MD95-2010 915-916
851 cm to the glass-based characterisation of FMAZ IV (JM11-19PC 542-543 cm) from Griggs et
852 al. (2014). All geochemical data plotted on a normalised anhydrous basis.

853

854 **Figure 6:** (a) (i) Percentage abundance of *Neogloboquadrina pachyderma* (sinistral) and (ii)
855 brown glass shard tephrostratigraphy incorporating 5 cm and 1 cm counts for the MD04-2822
856 core. (b) (i) Percentage abundance of *Neogloboquadrina pachyderma* (sinistral) and (ii)
857 brown glass shard tephrostratigraphy incorporating 5 cm and 1 cm counts for the MD04-
858 2829CQ core. Foram abundances and Dansgaard-Oeschger event numbering for MD04-2822
859 and MD04-2829CQ from Hibbert et al. (2010) and Hall et al. (2011) respectively. (c)
860 Geochemical characterisations of glass shards from Type 1 tephra deposits in the MD04-2822
861 and MD04-2829CQ cores. (i) inset of total alkali vs. silica plot. Division line to separate
862 alkaline and sub-alkaline material from MacDonald and Katsura (1964). Chemical
863 classification and nomenclature after Le Maitre et al. (1989). (ii) FeO/TiO₂ vs. SiO₂ and (iii)
864 TiO₂ vs. Al₂O₃ compositional variations diagrams comparing the glass shard composition of
865 MD04-2822 and MD04-2829CQ deposits to characterisations of proximal Icelandic material.
866 Geochemical fields for Icelandic source volcanoes are based on normalised whole rock and
867 glass shard analyses utilised in Bourne et al. (2015) and references within and additional data
868 for the Kverkfjöll volcano from Gudmundsdóttir et al. (2016). All geochemical data plotted
869 on a normalised anhydrous basis.

870

871 **Figure 7:** (a) (i) Percentage abundance of *Neogloboquadrina pachyderma* (sinistral), (ii) ash
872 free IRD concentration and (iii) tephrostratigraphic record of the MD99-2251 marine core.
873 Glass shard counts have been truncated for clarity. Shard counts in the 1686-1687 cm sample
874 (*) are 4991, 1862 and 507 shards per 0.5 g dws in the 25-80, 80-125 and >125 µm grain-size
875 fractions, respectively. The shard counts for the 25-80 µm grain-size fraction from the 1904-
876 1905 cm sample (**) are 3776 shards per 0.5 g dws. Red bars denote samples depths from
877 which glass shards were subsequently extracted for compositional characterisation. (b)
878 Composition of significant geochemical populations identified in glass analyses of tephra
879 deposits within the MD99-2251 core. (i) inset of total alkali vs. silica plot. Division line to
880 separate alkaline and sub-alkaline material from MacDonald and Katsura (1964). Chemical
881 classification and nomenclature after Le Maitre et al. (1989). (ii) FeO/TiO₂ vs. SiO₂ and (iii)

882 TiO₂ vs. Al₂O₃ compositional variations diagrams comparing significant glass shard based
883 geochemical populations from the MD99-2251 deposits to characterisations of proximal
884 Icelandic material. Geochemical fields for Icelandic source volcanoes are based on
885 normalised whole rock and glass shard analyses utilised in Bourne et al. (2015) and
886 references within and additional data for the Kverkfjöll volcano from Gudmundsdóttir et al.
887 (2016). All geochemical data plotted on a normalised anhydrous basis.

888

889 **Figure 8:** (a) (i) Percentage abundance of *Neogloboquadrina pachyderma* (sinistral), (ii)
890 percentage IRD (>150 µm fraction) and (iii) tephrostratigraphic record of the GIK23415-9
891 marine core. *Np*(s) and IRD data from Vogelsang et al. (2004) and Weinelt (2004),
892 respectively. Labels for Heinrich Events from Weinelt et al. (2003) and Lu et al. (2007).
893 Shard counts have been truncated for clarity. Shard counts in the 193-194 cm sample are
894 5131 and 280 shards per 0.5 g dws in the 25-80 and >125 µm grain-size fractions
895 respectively. Red bars denote samples depths from which glass shards were subsequently
896 extracted for compositional characterisation. (b) Composition of significant glass-based
897 geochemical populations identified in tephra deposits within the GIK23415-9 core. (i) inset
898 of total alkali vs. silica plot. Division line to separate alkaline and sub-alkaline material from
899 MacDonald and Katsura (1964). Chemical classification and nomenclature after Le Maitre et
900 al. (1989). (ii) FeO/TiO₂ vs. SiO₂ and (iii) TiO₂ vs. Al₂O₃ compositional variations diagrams
901 comparing significant glass-based geochemical populations from the GIK23415-9 deposits to
902 characterisations of proximal Icelandic material. Geochemical fields for Icelandic source
903 volcanoes are based on normalised whole rock and glass shard analyses utilised in Bourne et
904 al. (2015) and references within and additional data for the Kverkfjöll volcano from
905 Gudmundsdóttir et al. (2016). All geochemical data plotted on a normalised anhydrous basis.

906

907 **Figure 9:** (a) Comparison of the glass analyses of the MD04-2822 1836-1837 cm tephra
908 horizon and the GIK23415-9 225-226 cm (TAB-2) geochemical population. (b) Comparison
909 of the glass analyses of the FMAZ II tephra horizon (JM11-19PC 202-203 cm from Griggs et
910 al. (2014)) and that of the GIK23415-9 202-203 cm (THOL-1) geochemical population. All
911 geochemical data plotted on a normalised anhydrous basis.

912 **Supplementary Information**

913

914 *Supplementary Figures*

915

916 **Figures S1-S13:** Graphical analysis of geochemical populations identified within single-
917 shard major element glass analyses from tephra deposits within the MD99-2251 (S1-S7) and
918 GIK23415-9 (S8-S13) cores.

919

920 *Supplementary Data*

921

922 **Table S1:** Original major oxide concentrations of glass shards from deposits related to the
923 rhyolitic component of North Atlantic Ash Zone II (II-RHY-1). Deposits analysed are (i)
924 MD04-2822 2168-2169 cm (ii) MD95-2024 1445-1446 cm (iii) MD99-2251 1974-1975 cm
925 (supplementary peak) (iv) MD99-2251 2014-2015 cm (main peak) (v) M23485-1 622-623
926 cm (vi) GIK23415-9 429-430 cm (vii) MD01-2461 942-943 cm (supplementary peak) (viii)
927 MD01-2461 947-948 cm (main peak) (ix) MD04-2820CQ 610-611 cm (x) JM11-19PC 618-
928 623 cm (xi) MD95-2010 996-1000 cm.

929

930 **Table S2:** Similarity coefficient comparisons of average concentrations of glass analyses of
931 the II-RHY-1 component in deposits from cores analysed within this work and by Kvamme et
932 al. (1989), Austin et al. (2004), Wastegård et al. (2006) and Brendryen et al. (2011).

933

934 **Table S3:** Original major oxide concentrations of glass shards from basaltic and intermediate
935 shards directly associated with deposits of the rhyolitic component of North Atlantic Ash
936 Zone II (II-RHY-1). Deposits analysed are (i) MD99-2251 2014-2015 cm (ii) M23485-1 622-
937 623 cm (iii) GIK23415-9 429-430 cm (iv) MD01-2461 947-948 cm (v) MD04-2820CQ 610-
938 611 cm (vi) JM11-19PC 618-623 cm.

939

940 **Table S4:** Original major oxide concentrations of glass shards from the MD95-2010 915-916
941 cm tephra deposit.

942

943 **Table S5:** Original major oxide concentrations of glass shards from tephra deposits in the
944 MD04-2822 core. Deposits analysed are from the depths of (i) 1836-1837 cm (ii) 2004-2005
945 cm and (iii) 2017-2018 cm.

946

947 **Table S6:** Original major oxide concentrations of glass shards from tephra deposits in the
948 MD04-2829CQ core. Deposits analysed are from the depths of (i) 800-801 cm (ii) 930-931
949 cm and (iii) 934-935 cm.

950

951 **Table S7:** Original major oxide concentrations of glass shards from tephra deposits in the
952 MD04-2820CQ core. Deposits analysed are from the depths of (i) 487-488 cm (ii) 497-498
953 cm and (iii) 524-525 cm.

954

955 **Table S8:** Original major oxide concentrations of glass shards from tephra deposits in the
956 MD99-2251 core. Deposits analysed are from the depths of (i) 1654-1655 cm (ii) 1680-1681
957 cm (iii) 1683-1684 cm (iv) 1713-1714 cm (v) 1772-1773 cm (vi) 1796-1797 cm (vii) 1812-
958 1813 cm and (viii) 1904-1905 cm.

959

960 **Table S9:** Analysis of glass-based geochemical populations present within tephra deposits
961 identified in the MD99-2251 marine core. n = total number of analyses from deposits. Veid.-
962 Bárd. = Veidivötn-Bárdarbunga.

963

964 **Table S10:** Original major oxide concentrations of glass shards from tephra deposits in the
965 GIK23415-9 core. Deposits analysed are from the depths of (i) 173-174 cm (ii) 193-194 cm
966 (iii) 202-203 cm (iv) 225-226 cm (v) 302-303 cm (vi) 305-306 cm and (vii) 375-376 cm.

967

968 **Table S11:** Analysis of glass-based geochemical populations present within tephra deposits
969 identified in the GIK23415-9 marine core. n = total number of analyses from deposits. Veid.-
970 Bárd. = Veidivötn-Bárdarbunga.

971

972 **Table S12a:** Original secondary standard analyses of the BCR2g standard made throughout
973 analytical periods during which glass sample analyses presented in this work were analysed.

974

975 **Table S12b:** Original secondary standard analyses of the Lipari standard made throughout
976 analytical periods during which glass sample analyses presented in this work were analysed.

977

978 **Table S13:** Similarity coefficient comparisons between the glass-based geochemical
979 signatures of isochronous horizons and significant glass-based geochemical populations in

980 the marine tephra framework for the North Atlantic between 25-60 ka BP. Method of
981 Borhardt et al. (1972) utilised. Red text shows SC values between 0.97 and 0.999 grey text
982 shows SC values less than 0.95.

983 **References**

984

985

986 Abbott, P.M., Austin, W.E.N., Davies, S.M., Pearce, N.J.G., Hibbert, F.D., 2013.
987 Cryptotephrochronology of a North East Atlantic marine sequence over Termination II, the
988 Eemian and the last interglacial-glacial transition. *Journal of Quaternary Science* 28, 501-514.

989

990 Abbott, P.M., Austin, W.E.N., Davies, S.M., Pearce, N.J.G., Rasmussen, T.L., Wastegård, S.,
991 Brendryen, J., 2014. Re-evaluation and extension of the MIS 5 tephrostratigraphy of the
992 Faroe Islands Region: the cryptotephra record. *Palaeogeography, Palaeoclimatology,*
993 *Palaeoecology* 409, 153-168.

994

995 Abbott, P.M., Bourne, A.J., Purcell, C.S., Davies, S.M., Scourse, J.D., Pearce, N.J.G., 2016.
996 Last Glacial Period Cryptotephra deposits in an eastern North Atlantic marine sequence:
997 Exploring linkages to the Greenland ice-cores. *Quaternary Geochronology* 31, 62-76.

998

999 Abbott, P.M., Davies, S.M., 2012. Volcanism and the Greenland ice-cores: the tephra record.
1000 *Earth-Science Reviews* 115, 173-191.

1001

1002 Abbott, P.M., Davies, S.M., Austin, W.E.N., Pearce, N.J.G., Hibbert, F.D., 2011.
1003 Identification of cryptotephra horizons in a North East Atlantic marine record spanning
1004 marine isotope stages 4 and 5a (~60,000-82,000 a b2k). *Quaternary International* 246, 177-
1005 189.

1006

1007 Abbott, P.M., Griggs, A.J., Bourne, A.J., Davies, S.M., in revision. Tracing marine
1008 cryptotephra in the North Atlantic during the Last Glacial Period: Protocols for
1009 identification, characterisation and evaluating depositional controls. Submitted to *Marine*
1010 *Geology*.

1011

1012 Austin, W.E.N., Abbott, P.M., 2010. Comment: Were last glacial climate events
1013 simultaneous between Greenland and France? A quantitative comparison using non-tuned
1014 chronologies. M. Blaauw, B. Wohlfarth, J.A. Christen, L. Ampel, D. Veres, K. Hughen, F.
1015 Preusser and A. Svensson (2009). *Journal of Quaternary Science* 25, 1045-1046.

1016

1017 Austin W.E.N., Wilson L.J., Hunt J.B., 2004. The age and chronostratigraphical significance
1018 of North Atlantic Ash Zone II. *Journal of Quaternary Science* 19, 137-146.

1019

1020 Aymerich, I.F., Oliva, M., Giralt, S., Martin-Herrero, 2016. Detection of Tephra Layers in
1021 Antarctic Sediment cores with Hyperspectral Imaging. *PLoS ONE* 11(1): e0146578.
1022 doi:10.1371/journal.pone.0146578.

1023

1024 Blockley, S.P.E., Bourne, A.J., Brauer, A., Davies, S.M., Hardiman, M., Harding, P.R., Lane,
1025 C.S., MacLeod, A., Matthews, I.P., Pyne-O'Donnell, S.D.F., Rasmussen, S.O., Wulf, S.,
1026 Zanchetta, G., 2014. Tephrochronology and the extended intimate (integration of ice-core,
1027 marine and terrestrial records) event stratigraphy 8-128 ka b2k. *Quaternary Science Reviews*
1028 106, 88-100.

1029

1030 Bond, G., Broecker, W., Johnsen, S., McManus, J., Labeyrie, L., Jouzel, J., Bonani, G., 1993.
1031 Correlations between climate records from North Atlantic sediments and Greenland ice.
1032 *Nature* 365, 143-147.

1033

1034 Borchardt, G.A., Aruscavage, P.J., Millard, H., 1972. Correlation of the Bishop ash, a
1035 Pleistocene marker bed, using instrumental neutron activation analysis. *Journal of*
1036 *Sedimentary Petrology* 42, 201-206.

1037

1038 Bourne, A.J., Davies, S.M., Abbott, P.M., Rasmussen, S.O., Steffensen, J.P., Svensson, A.,
1039 2013. Revisiting the Faroe Marine Ash Zone III in two Greenland ice cores: implications for
1040 marine-ice correlations. *Journal of Quaternary Science* 28, 641-646.

1041

1042 Bourne, A.J., Cook, E., Abbott, P.M., Seierstad, I.K., Steffensen, J.P., Svensson, A., Fischer,
1043 H., Schupbach, S., Davies, S.M., 2015. A tephra lattice for Greenland and a reconstruction of
1044 volcanic events spanning 25-45 ka b2k. *Quaternary Science Reviews* 118, 122-141.

1045

1046 Bramlette M.N., Bradley W.H., 1941. Geology and biology of North Atlantic deep-sea cores
1047 between Newfoundland and Ireland: I. Lithology and geologic interpretation. U.S. Geological
1048 Survey Professional Paper 196-A, 1-34.

1049

1050 Brendryen, J., Haflidason, H., Sejrup, H.P., 2010. Norwegian Sea tephrostratigraphy of
1051 marine isotope stages 4 and 5: Prospects and problems for tephrochronology in the North
1052 Atlantic region. *Quaternary Science Reviews* 29, 847-864.

1053

1054 Brendryen, J., Haflidason, H., Sejrup, H.P., 2011. Non-synchronous deposition of North
1055 Atlantic Ash Zone II in Greenland ice cores, and North Atlantic and Norwegian Sea
1056 sediments: an example of complex glacial-stage tephra transport. *Journal of Quaternary*
1057 *Science* 26, 739-745.

1058

1059 D'Anjou, R.M., Balascio, N.L., Bradley, R.S., 2014. Locating cryptotephra in lake sediments
1060 using fluid imaging technology. *Journal of Paleolimnology* 52, 257-264.

1061

1062 Davies, S.M., 2015. Cryptotephra: the revolution in correlation and precision dating. *Journal*
1063 *of Quaternary Science* 30, 114-130.

1064

1065 Davies, S.M., Abbott, P.M., Meara, Rh. H., Pearce, N.J.G., Austin, W.E.N., Chapman, M. R.,
1066 Svensson, A., Bigler, M., Rasmussen, T.L., Rasmussen, S.O., Farmer, E.J., 2014. A North
1067 Atlantic tephrostratigraphical framework for 130-60 ka b2k: new tephra discoveries, marine-
1068 based correlations, and future challenges. *Quaternary Science Reviews* 106, 101-121.

1069

1070 Davies, S.M., Abbott, P.M., Pearce, N.J.G., Wastegård, S., Blockley, S.P.E., 2012.
1071 Integrating the INTIMATE records using tephrochronology: rising to the challenge.
1072 *Quaternary Science Reviews* 36, 11-27.

1073

1074 Davies, S.M., Wastegård, S., Abbott, P.M., Barbante, C., Bigler, M., Johnsen, S.J.,
1075 Rasmussen, T.L., Steffensen, J.P., Svensson, A., 2010. Tracing volcanic events in the NGRIP
1076 ice-core and synchronising North Atlantic marine records during the last glacial period. *Earth*
1077 *and Planetary Science Letters* 294, 69-79.

1078

1079 Davies, S.M., Wastegård, S., Rasmussen, T.L., Svensson, A., Johnsen, S.J., Steffensen, J.P.,
1080 Andersen, K.K., 2008. Identification of the Fugloyarbanki tephra in the NGRIP ice core: a
1081 key tie-point for marine and ice-core sequences during the last glacial period. *Journal of*
1082 *Quaternary Science* 23, 409-414.

1083
1084 Dokken, T.M., Jansen, E., 1999. Rapid changes in the mechanism of ocean convection during
1085 the last glacial period. *Nature* 401, 458-461.
1086
1087 Griggs, A.J., Davies, S.M., Abbott, P.M., Coleman, M., Palmer, A.P., Rasmussen, T.L.,
1088 Johnston, R., 2015. Visualising tephra sedimentation processes in the marine environment:
1089 the potential of X-ray microtomography. *Geochemistry, Geophysics, Geosystems* 16, doi:
1090 10.1002/2015GC006073.
1091
1092 Griggs, A.J., Davies, S.M., Abbott, P.M., Rasmussen, T.L., Palmer, A.P., 2014. Optimising
1093 the use of marine tephrochronology in the North Atlantic: A detailed investigation of the
1094 Faroe Marine Ash Zones II, III and IV. *Quaternary Science Reviews* 106, 122-139.
1095
1096 Grönvold K., Óskarsson N., Johnsen S.J., Clausen H.B., Hammer C.U., Bond G., Bard E.,
1097 1995. Ash layers from Iceland in the Greenland GRIP ice core correlated with oceanic and
1098 land sediments. *Earth and Planetary Science Letters* 135, 149-155.
1099
1100 Gudmundsdóttir, E.R., Larsen, G., Björck, S., Ingólfsson, Ó., Striberger, J., 2016. A new
1101 high-resolution tephra stratigraphy in eastern Iceland: Improving the Icelandic and North
1102 Atlantic tephrochronology. *Quaternary Science Reviews* 150, 234-249.
1103
1104 Haflidason H., Eiriksson J., Van Kreveld S., 2000. The tephrochronology of Iceland and the
1105 North Atlantic region during the Middle and Late Quaternary: a review. *Journal of*
1106 *Quaternary Science* 15, 3-22.
1107
1108 Hall, I.R., Colmenero-Hidalgo, E., Zahn, R., Peck, V.L., Hemming, S.R., 2011. Centennial-
1109 to millennial-scale ice-ocean interactions in the subpolar northeast Atlantic 18-41 kyr ago.
1110 *Paleoceanography* 26, PA2224, doi:10.1029/2010PA002084.
1111
1112 Henry, L.G., McManus, J.F., Curry, W.B., Roberts, N.L., Piotrowski, A.M., Keigwin, L.D.,
1113 2016. North Atlantic ocean circulation and abrupt climate change during the last glaciation.
1114 *Science* 353, 470-474.
1115
1116 Hibbert, F.D., Austin, W.E.N., Leng, M.J., Gatliff, R.W., 2010. British Ice Sheet dynamics
1117 inferred from North Atlantic ice-rafted debris records spanning the last 175 000 years.
1118 *Journal of Quaternary Science* 25, 461-482.
1119
1120 Hunt, J.B., Hill, P.G., 2001. Tephrological implications of beam size-sample-size effects in
1121 electron microprobe analysis of glass shards. *Journal of Quaternary Science* 16, 105-117.
1122
1123 Jørgensen, K.A., 1980. The Thorsmörk ignimbrite: An unusual comenditic pyroclastic flow
1124 in Southern Iceland. *Journal of Volcanology and Geothermal Research* 8, 7-22.
1125
1126 Kolling, H., Bauch, H. A., 2017. A Stratigraphical-Sedimentological Study of the Last
1127 Interglacial Period in the Central Nordic Seas on the Basis of XRF Core Scanning.
1128 *Polarforschung* 87, 15-22.
1129
1130 Kuehn, S.C., Froese, D.G., Shane, P.A.R., INTAV Intercomparison Participants (2011) “The
1131 INTAV intercomparison of electron-beam microanalysis of glass by tephrochronology
1132 laboratories: Results and recommendations”, *Quaternary International* 246, 19-47.

1133
1134 Kvamme T, Mangerud J, Furnes H, Ruddiman W., 1989. Geochemistry of Pleistocene ash
1135 zones in cores from the North Atlantic. *Norsk Geologisk Tidsskrift* 69, 251-272.
1136
1137 Lacasse C, Sigurdsson H, Carey S, Paterne M, Guichard F., 1996. North Atlantic deep-sea
1138 sedimentation of Late Quaternary tephra from the Iceland hotspot. *Marine Geology* 129, 207-
1139 235.
1140
1141 Lackschewitz, K.S., Wallrabe-Adams, H.-J., 1997. Composition and origin of volcanic ash
1142 zones in Late Quaternary sediments from the Rekjanes Ridge: evidence for ash fallout and
1143 ice-rafting. *Marine Geology* 136, 209-224.
1144
1145 Lane, C.S., Brauer, A., Blockley, S.P.E., Dulski, P., 2013. Volcanic ash reveals time-
1146 transgressive abrupt climate change during the Younger Dryas. *Geology* 41, 1251-1254.
1147
1148 Le Maitre, R.W., Bateman, P., Dudek, A., Keller, J., Lameyre, Le Bas, M.J., Sabine, P.A.,
1149 Schmid, R., Sorensen, H., Streckeisen, A., Woolley, A.R., Zanettin, B., 1989. A
1150 Classification of Igneous Rocks and Glossary of Terms. Blackwell, Oxford.
1151
1152 Lowe, D.J., 2011. Tephrochronology and its application: A review. *Quaternary*
1153 *Geochronology* 6, 107-153.
1154
1155 Lowe, D.J., Pearce, N.J.G., Jorgensen, M.A., Kuehn, S.C., Tryon, C.A., Hayward, C.L.,
1156 2017. Correlating tephras and cryptotephras using glass compositional analyses and
1157 numerical and statistical methods: Review and evaluation. *Quaternary Science Reviews* 175,
1158 1-44.
1159
1160 Lowe, D.J., Shane, P.A.R., Alloway, B.V., Newnham, R.M., 2008. Fingerprints and age
1161 models for widespread New Zealand tephra marker beds erupted since 30,000
1162 years ago: a framework for NZ-INTIMATE. *Quaternary Science Reviews* 27, 95-126.
1163
1164 Lowe, J.J., Barton, N., Blockley, S., Bronk Ramsey, C., Cullen, V.L., Davies, W., Gamble,
1165 C., Grant, K., Hardiman, M., Housley, R., Lane, C.S., Lee, S., Lewis, M., MacLeod, A.,
1166 Menzies, M., Müller, W., Pollard, M., Price, C., Roberts, A.P., Rohling, E.J., Satow, C.,
1167 Smith, V.C., Stringer, C.B., Tomlinson, E.L., White, D., Albert, P., Arienzo, I., Barker, G.,
1168 Borić, D., Carandente, A., Civetta, L., Ferrier, C., Guadelli, J.-L., Karkanis, P., Koumouzelis,
1169 M., Müller, U.C., Orsi, G., Pross, J., Rosi, M., Shalamanov-Korobar, L., Sirakov, N.,
1170 Tzedakis, P.C., 2012. Volcanic ash layers illuminate the resilience of Neanderthals and early
1171 modern humans to natural hazards. *Proceedings of the National Academy of Sciences* 109,
1172 13532-13537.
1173
1174 Lowe, J.J., Bronk Ramsey, C., Housley, R.A., Lane, C.S., Tomlinson, E.L., RESET Team,
1175 RESET Associates, 2015. The RESET project: constructing a European tephra lattice for
1176 refined synchronisation of environmental and archaeological events during the last c. 100 ka.
1177 *Quaternary Science Reviews* 118, 1-17.
1178
1179 Lowe, J.J., Rasmussen, S.O., Björck, S., Hoek, W.Z., Steffensen, J.P., Walker, M.J.C., Yu,
1180 Z.C., the INTIMATE group, 2008. Synchronisation of palaeoenvironmental events in the
1181 North Atlantic region during the Last Termination: a revised protocol recommended by the
1182 INTIMATE group. *Quaternary Science Reviews* 27, 6-17.

1183
1184 Lu, H.-Y., Wu, N.-Q., Liu, K.-B., Jiang, H., Liu, T.-S., 2007. Phytoliths as quantitative
1185 indicators for the reconstruction of past environmental conditions in China II:
1186 palaeoenvironmental reconstruction in the Loess Plateau. *Quaternary Science Reviews* 26,
1187 759-772.

1188
1189 MacDonald, G.A., Katsura, T. 1964. Chemical composition of Hawaiian lavas. *Journal of*
1190 *Petrology* 5, 83-133.

1191
1192 Martrat, B., Grimalt, J.O., Shackleton, N.J., de Abreu, L., Hutterli, M.A. and Stocker, T.F.,
1193 2007. Four climate cycles of recurring deep and surface water destabilizations on the Iberian
1194 Margin. *Science* 317, 502-507.

1195
1196 Matthews, I.P., Trincardi, F., Lowe, J.J., Bourne, A.J., Macleod, A., Abbott, P.M., Andersen,
1197 N., Asioli, A., Blockley, S.P.E., Lane, C.S., Oh, Y.A., Satow, C.S., Staff, R.A., Wulf, S.,
1198 2015. Developing a robust tephrochronological framework for Late Quaternary marine
1199 records in the Southern Adriatic Sea: new data from core station SA03-11. *Quaternary*
1200 *Science Reviews* 118, 84-104.

1201
1202 Mortensen, A.K., Bigler, M., Grönvold, K., Steffensen, J.P., Johnsen, S.J., 2005. Volcanic
1203 ash layers from the Last Glacial Termination in the NGRIP ice core. *Journal of Quaternary*
1204 *Science* 20, 209-219.

1205
1206 North Greenland Ice Core Project Members, 2004. High-resolution record of Northern
1207 Hemisphere climate extending into the last interglacial period. *Nature* 431, 147-151.

1208
1209 Óladóttir, B.A., Sigmarsson, O., Larsen, G., Devidal, J.-L., 2011. Provenance of basaltic
1210 tephra from Vatnajökull subglacial volcanoes, Iceland, as determined by major- and trace-
1211 element analyses. *The Holocene* 21, 1037-1048.

1212
1213 Rasmussen, T.L., Wastegård, S., Kuijpers, A., van Weering, T.C.E., Heinemeier, J.,
1214 Thomsen, E., 2003. Stratigraphy and distribution of tephra layers in marine sediment cores
1215 from the Faeroe Islands, North Atlantic. *Marine Geology* 199, 263-277.

1216
1217 Ruddiman W., Glover R., 1972. Vertical mixing of ice-rafted volcanic ash in North Atlantic
1218 sediments. *Geological Society Bulletin* 83, 2817-2836.

1219
1220 Sanchez Goñi, M.F., Harrison, S.P., 2010. Millennial-scale climate variability and vegetation
1221 changes during the Last Glacial: concepts and terminology. *Quaternary Science Reviews* 29,
1222 2823-2827.

1223
1224 Seierstad, I.K., Abbott, P.M., Bigler, M., Blunier, T., Bourne, A.J., Brook, E., Buchardt, S.L.,
1225 Buizert, C., Clausen, H.B., Cook, E., Dahl-Jensen, D., Davies, S.M., Guillevic, M., Johnsen,
1226 S.J., Pedersen, D.S., Popp, T.J., Rasmussen, S.O., Severinghaus, J.P., Svensson, A., Vinther,
1227 B.M. (2014). Consistently dated records from the Greenland GRIP, GISP2, and NGRIP ice
1228 cores for the past 104 ka reveal millennial-scale $\delta^{18}\text{O}$ gradients with possible Heinrich event
1229 imprint. *Quaternary Science Reviews* 106, 29-46.

1230
1231 Timms, R.G.O., Matthews, I.P., Palmer, A.P., Candy, I., Abel, L. (2017) A high-resolution
1232 tephrostratigraphy from Quoyloo Meadow, Orkney, Scotland: Implications for the

- 1233 tephrostratigraphy of NW Europe during the Last Glacial-Interglacial Transition. *Quaternary*
1234 *Geochronology* 40, 67-81.
- 1235
1236 Tryon, C.A., Logan, M.A.V., Mouralis, D., Kuehn, S., Slimak, L., Balkan-Atlı, N., 2009.
1237 Building a tephrostratigraphic framework for the Paleolithic of central Anatolia, Turkey.
1238 *Journal of Archaeological Science* 36, 637-652.
- 1239
1240 Voelker, A.H.L., Hafliðason, H., 2015. Refining the Icelandic tephrochronology of the last
1241 glacial period – The deep-sea core PS2644 record from the southern Greenland Sea. *Global*
1242 *and Planetary Change* 131, 35-62.
- 1243
1244 Vogelsang, E., Sarnthein, M., Pflaumann, U., 2004. Distribution of planktic foraminifera in
1245 sediment core GIK23415-9. DOI:10.1594/PANGAEA.186156.
- 1246
1247 Wastegård, S., Rasmussen, T.L., 2014. Faroe Marine Ash Zone IV: a new MIS 3 ash zone on
1248 the Faroe Islands margin. In Austin, W.E.N., Abbott, P.M., Davies, S.M., Pearce, N.J.G.,
1249 Wastegård, S., (eds) *Marine Tephrochronology*, Geological Society of London Special
1250 Publication 398, 81-93.
- 1251
1252 Wastegård S., Rasmussen T.L., Kuijpers A., Nielsen T., van Weering, T.C.E., 2006.
1253 Composition and origin of ash zones from Marine Isotope Stages 3 and 2 in the North
1254 Atlantic. *Quaternary Science Reviews* 25, 2409-2419.
- 1255
1256 Weinelt, M. (2004) Ice rafted debris of sediment core GIK23415-9.
1257 DOI:10.1594/PANGAEA.143869.
- 1258
1259 Zanchetta, G., Sulpizio, R., Roberts, N., Cioni, R., Eastwood, W.J., Siani, G., Caron, B.,
1260 Paterne, M., Santacrose, R., 2011. Tephrostratigraphy, chronology and climatic events of the
1261 Mediterranean basin during the Holocene: An overview. *The Holocene* 21, 33-52.
- 1262
1263 Zielinski G.A., Mayewski P.A., Meeker L.D., Gronvöld K., Germani M.S., Whitlow S.,
1264 Twickler M.S., Taylor K., 1997. Volcanic aerosol records and tephrochronology of the
1265 Summit, Greenland, ice cores. *Journal of Geophysical Research* 102, 26,625-26,640.
- 1266
1267 Zumaque, J., Eynaud, F., Zaragosi, S., Marret, F., Matsuzaki, K.M., Kissel, C., Roche, D.M.,
1268 Malaize, B., Michel, E., Billy, I., Richter, T., Palis, E., 2012. An ocean-ice coupled response
1269 during the last glacial: a view from a marine isotope stage 3 record south of the Faeroe
1270 Shetland Gateway. *Climate of the Past* 8, 1997-2017.

Table 1: Summary of isochronous horizons and significant geochemical populations forming the marine tephra framework for the North Atlantic between 25-60 ka BP. The designation of climatic events is based on pre-existing stratigraphic frameworks for the cores. The stratigraphic ordering of horizons between cores is approximate. FMAZ II, FMAZ IV and NAAZ II have been identified in multiple cores. H = Heinrich Event; DO = Dansgaard-Oeschger Event. bas = basaltic; rhy = rhyolitic. Vat. = Vatnafjöll; Veid.-Bárd. = Veidivötn-Bárdarbunga. Deposit types based on the classification scheme outlined in Abbott et al. (submitted). References are as follows: 1: this study; 2: Rasmussen et al. (2003); 3: Wastegård et al. (2006); 4: Davies et al. (2008); 5: Griggs et al. (2014); 6: Abbott et al. (2016); 7: Wastegård and Rasmussen (2014); 8: Kvamme et al. (1989); 9: Austin et al. (2004); 10: Brendryen et al. (2010).

Tephra horizon/deposit (pop.)	Climatic event	Composition	Volcanic source	Deposit type	Ref(s)
<i>Isochronous horizons</i>					
GIK23415-9 173-174 cm (THOL-1)	Post H2	Tholeiitic bas	Kverkfjöll	1	1
FMAZ II	Post DO-3	Transitional alkali bas	Hekla/Vatnafjöll	2A	2, 3, 4, 5
MD04-2822 1836-1837 cm	Pre DO-4	Transitional alkali bas	Katla or Hekla/Vatnafjöll	1	1
GIK23415-9 225-226 cm (TAB-1)	H3	Transitional alkali bas	Katla or Hekla/Vat.	1	1
MD04-2829CQ 800-801 cm (THOL-1)	Pre DO-4	Tholeiitic bas	Grímsvötn	1	1
MD04-2829CQ 800-801 cm (THOL-2)	Pre DO-4	Tholeiitic bas	Kverkfjöll	1	1
MD99-2251 1680-1681 cm (TAB-1)	H3	Transitional alkali bas	Katla	2A	1
MD04-2822 2004-2005 cm	DO-8	Transitional alkali bas	Katla	1	1
MD04-2829CQ 930-931 cm	DO-8	Tholeiitic bas	Grímsvötn	1	1
MD04-2829CQ 934-935 cm	Pre DO-8	Tholeiitic bas	Grímsvötn	1	1
MD04-2820CQ 487-488 cm	Pre DO-8 (H4)	Tholeiitic bas	Grímsvötn	2A	6
MD04-2820CQ 497-498 cm	Pre DO-9	Transitional alkali rhy	Katla	2A	6
MD04-2822 2017-2018 cm	Pre DO-9	Tholeiitic bas	Grímsvötn	1	1
MD04-2820CQ 524-525 cm	Pre DO-11	Tholeiitic bas	Grímsvötn or Kverkfjöll	2A	6
FMAZ IV	Pre DO-12	Tholeiitic bas	Grímsvötn	2A	5, 7
NAAZ II (II-RHY-1)	End of DO-15	Transitional alkali rhy	Tindfjallajökull	3	1, 3, 8, 9, 10
<i>Significant geochemical populations</i>					
GIK23415-9 202-203 cm (TAB-1)	Pre H2	Transitional alkali bas	Katla	2B	1
GIK23415-9 202-203 cm (THOL-1)	Pre H2	Tholeiitic bas	Kverkfjöll	2B	1
GIK23415-9 202-203 cm (THOL-2)	Pre H2	Tholeiitic bas	Grímsvötn	2B	1
GIK23415-9 202-203 cm (THOL-3)	Pre H2	Tholeiitic bas	Veid. -Bárd.	2B	1
MD99-2251 1713-1714 cm (TAB-1)	Pre H3	Transitional alkali bas	Katla	2B	1
MD99-2251 1713-1714 cm (THOL-1)	Pre H3	Tholeiitic bas	Grímsvötn	2B	1
MD99-2251 1772-1773 cm (TAB-1)	Post H4	Transitional alkali bas	Katla	2B	1
MD99-2251 1772-1773 cm (TAB-2)	Post H4	Transitional alkali bas	Katla (?)	2B	1
GIK23415-9 302-306 cm (THOL-1)	H4	Tholeiitic bas	Grímsvötn	4	1
GIK23415-9 302-306 cm (THOL-2)	H4	Tholeiitic bas	Grímsvötn (?)	4	1
MD99-2251 1812-1813 cm (THOL-1)	H4	Tholeiitic bas	Grímsvötn	2B	1
MD99-2251 1812-1813 cm (THOL-2)	H4	Tholeiitic bas	Veid. -Bárd.	2B	1
MD99-2251 1812-1813 cm (THOL-3)	H4	Tholeiitic bas	Veid. -Bárd.	2B	1
MD99-2251 1812-1813 cm (TAB-1)	H4	Transitional alkali bas	Katla	2B	1
MD99-2251 1904-1905 cm (ALK-1)	Post H5	Alkali bas	Vestmannaeyjar	2B	1
GIK23415-9 375-376 cm (THOL-1)	Pre H5	Tholeiitic bas	Grímsvötn	2B	1
NAAZ II (II-THOL-2)	End of DO-15	Tholeiitic bas	Grímsvötn	2A, 2B	8, 1
NAAZ II (II-TAB-1)	End of DO-15	Transitional alkali bas	Katla	2A, 2B	8, 1
NAAZ II (II-INT-1)	End of DO-15	Trachyandesite-Trachydacite	Unknown	2A, 2B	1

Figure 1

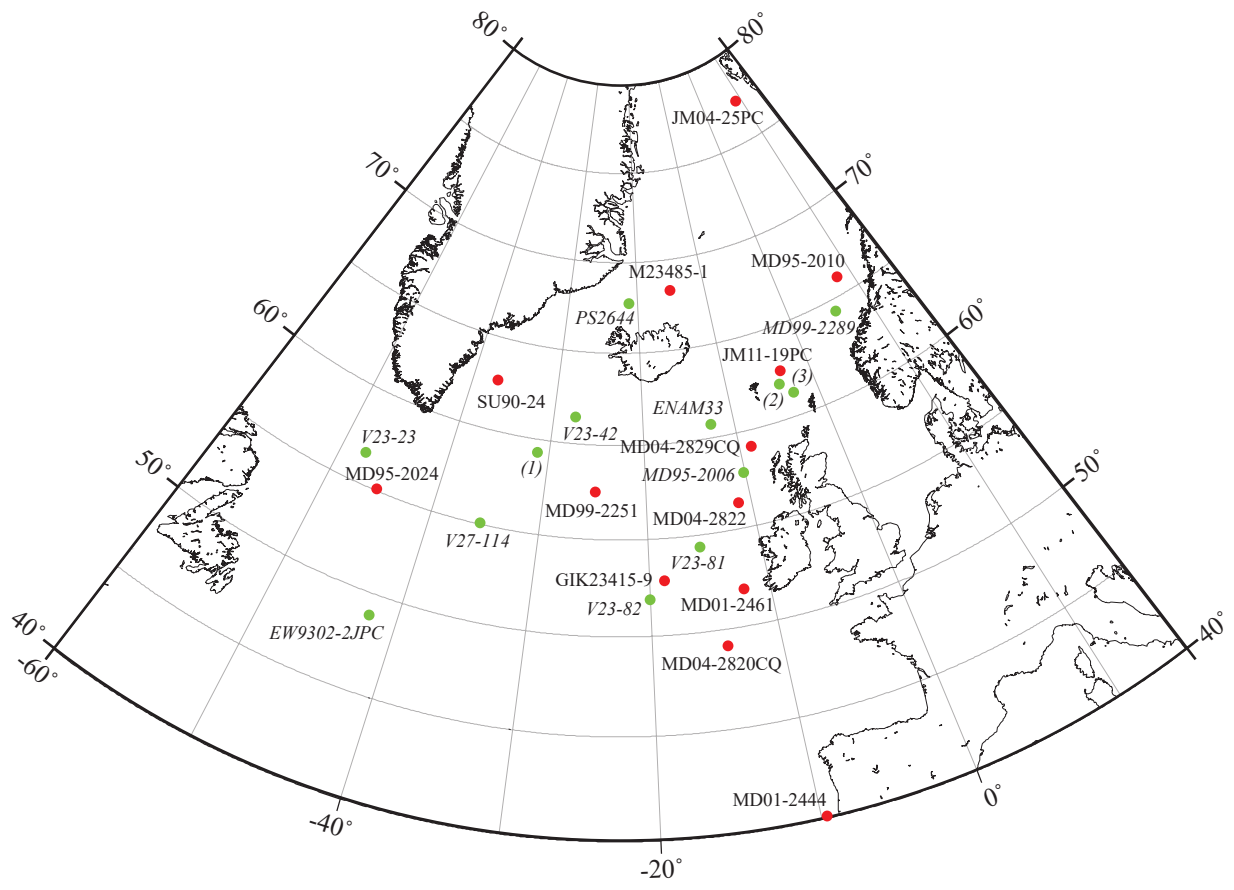
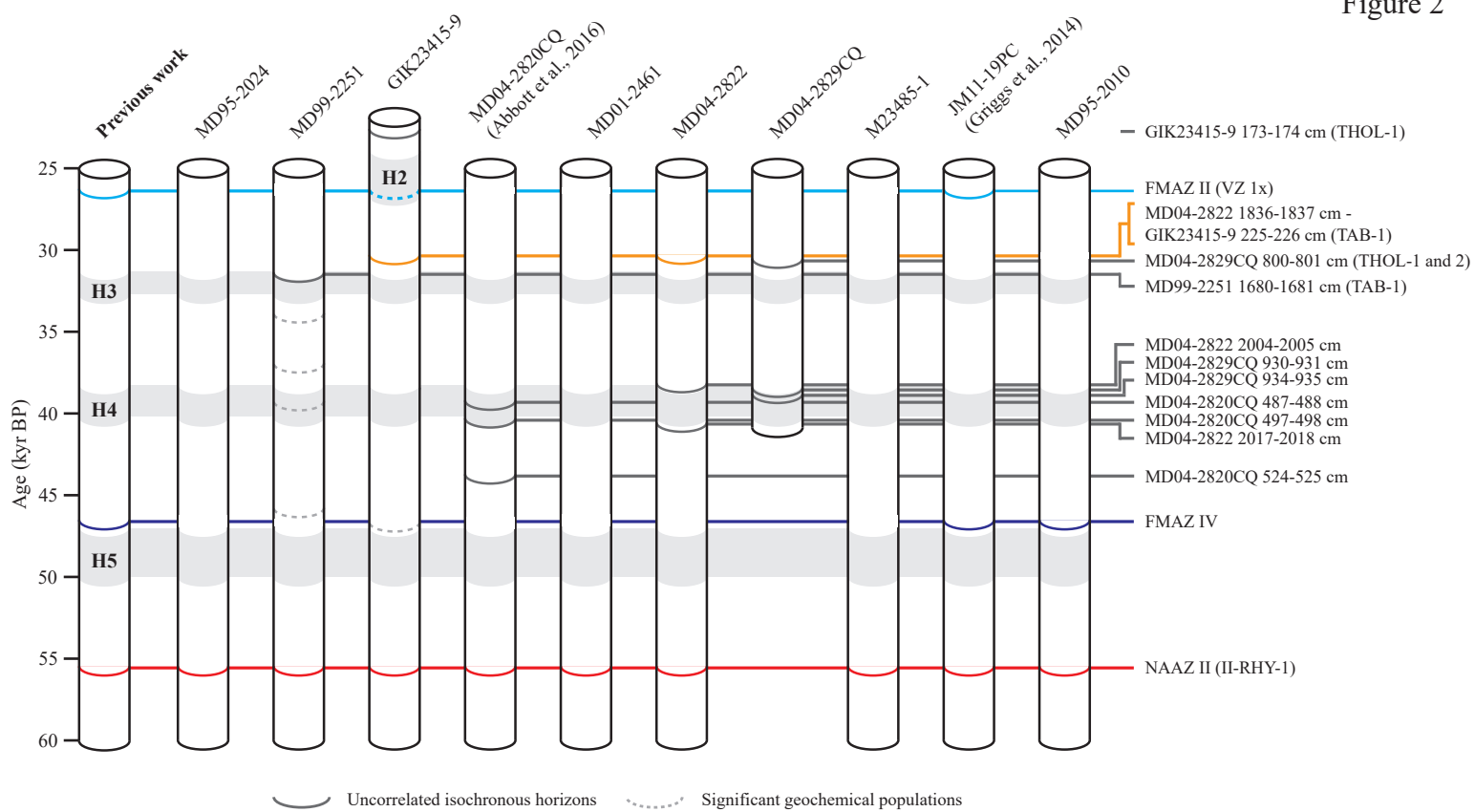
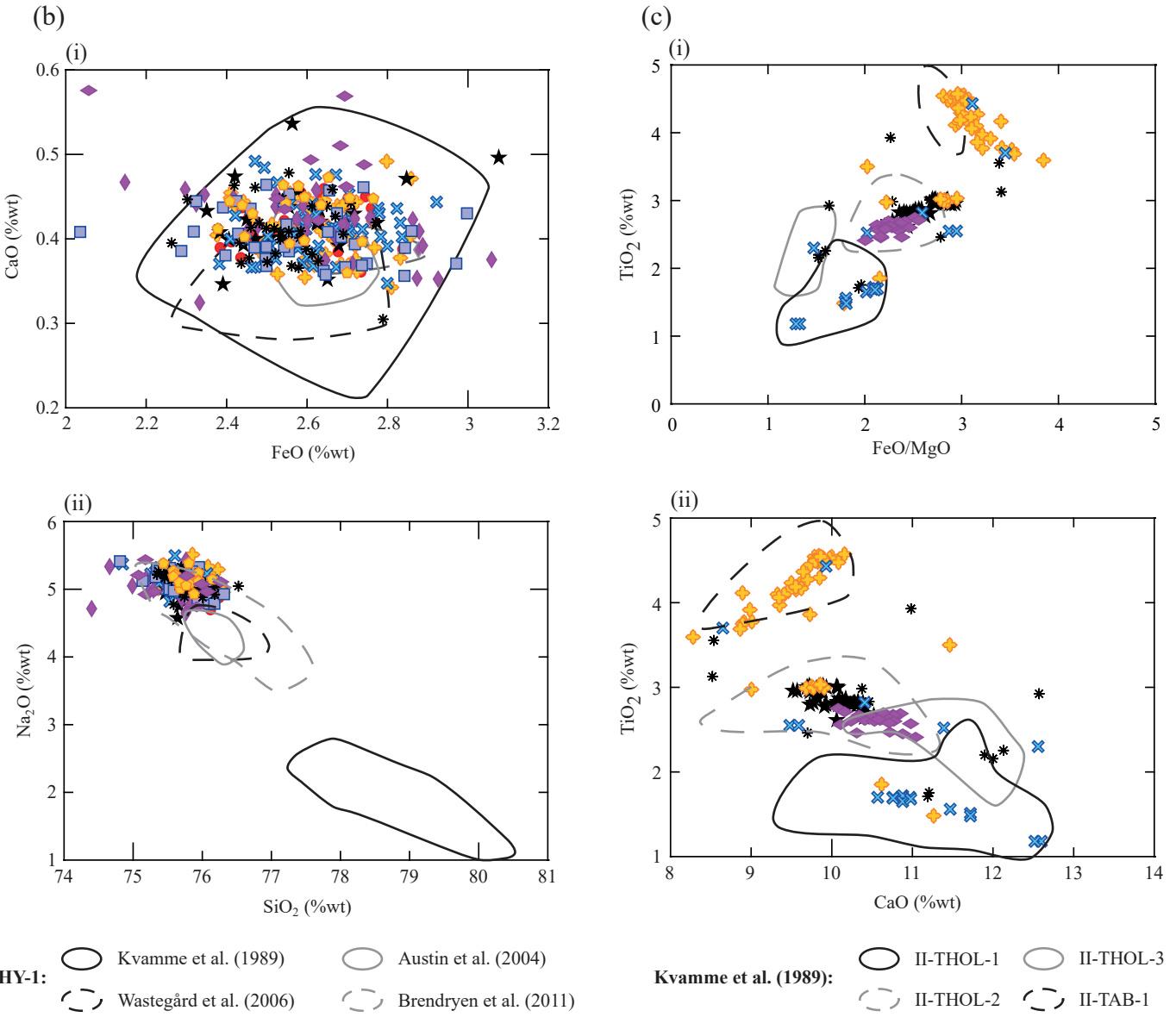
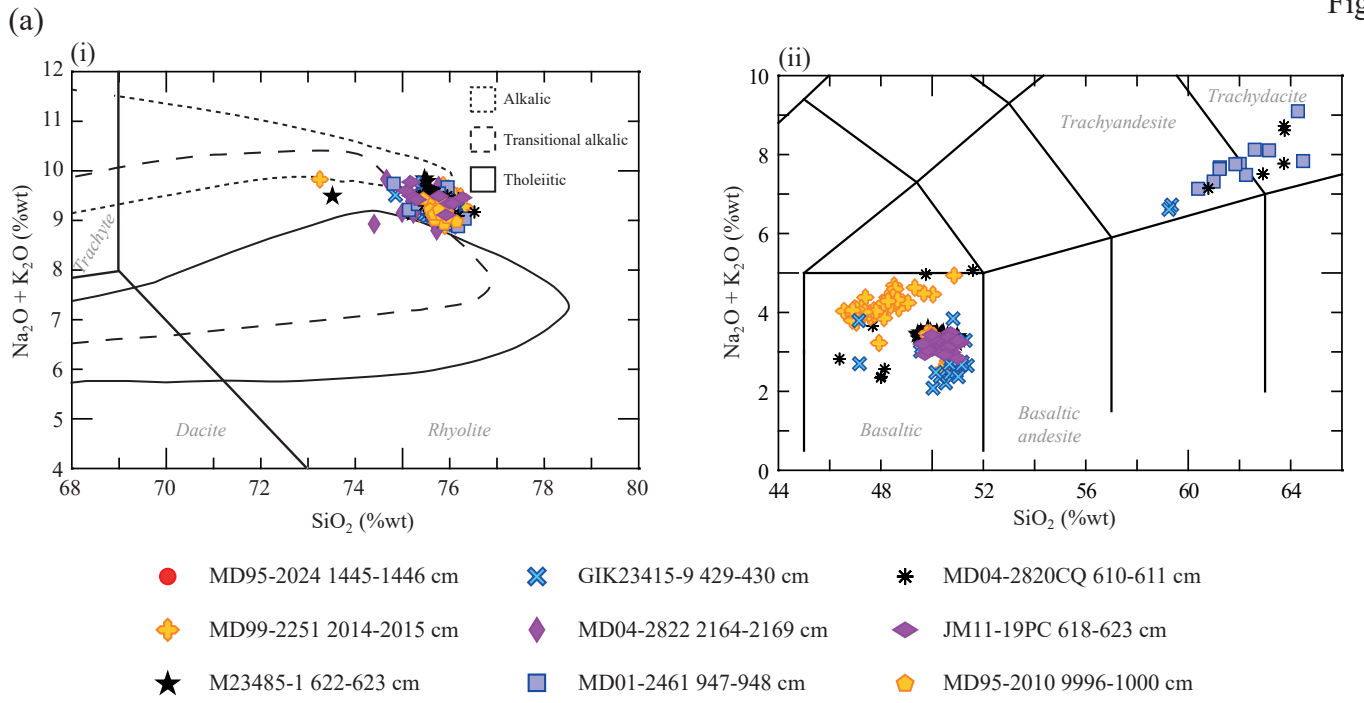
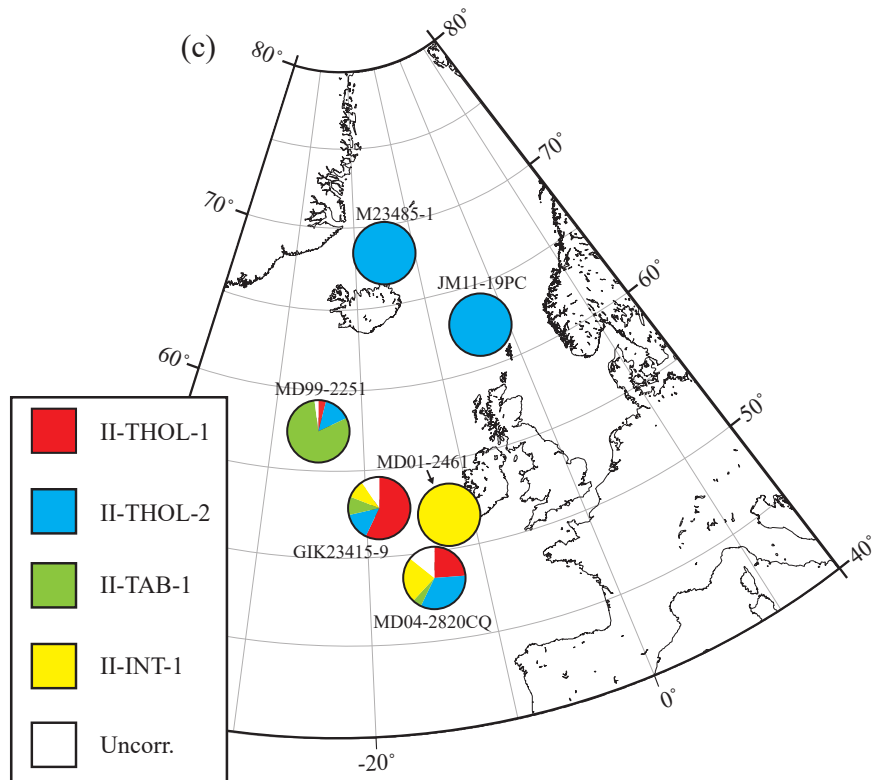
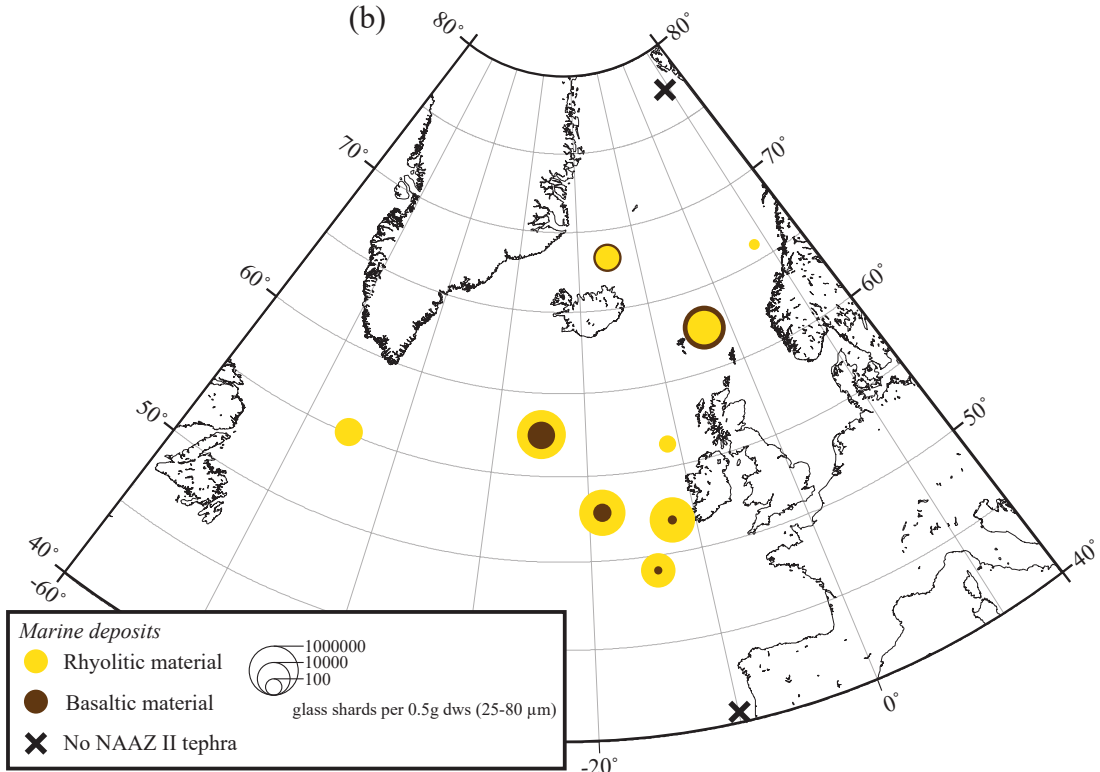
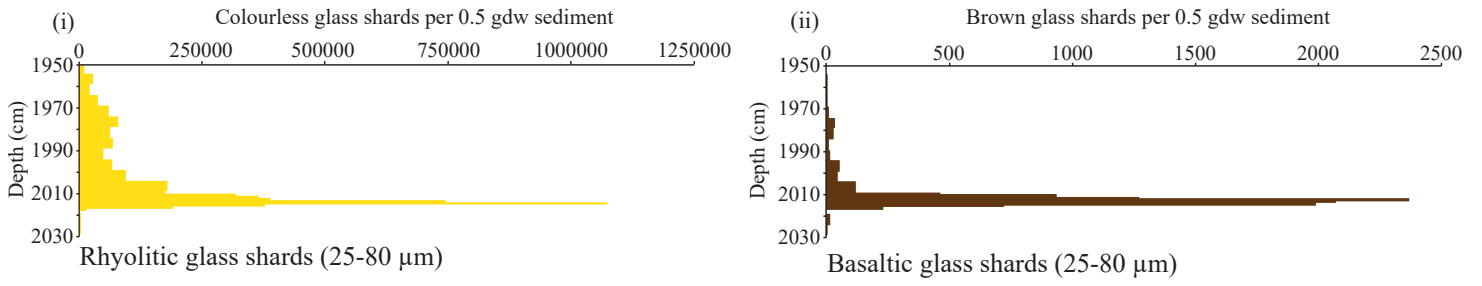


Figure 2

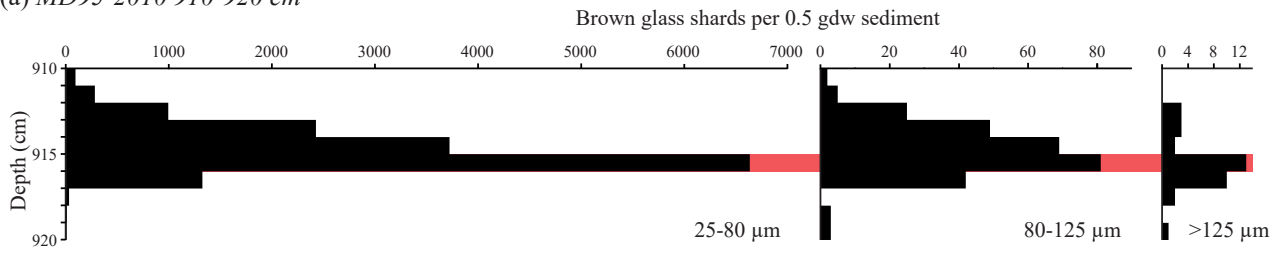




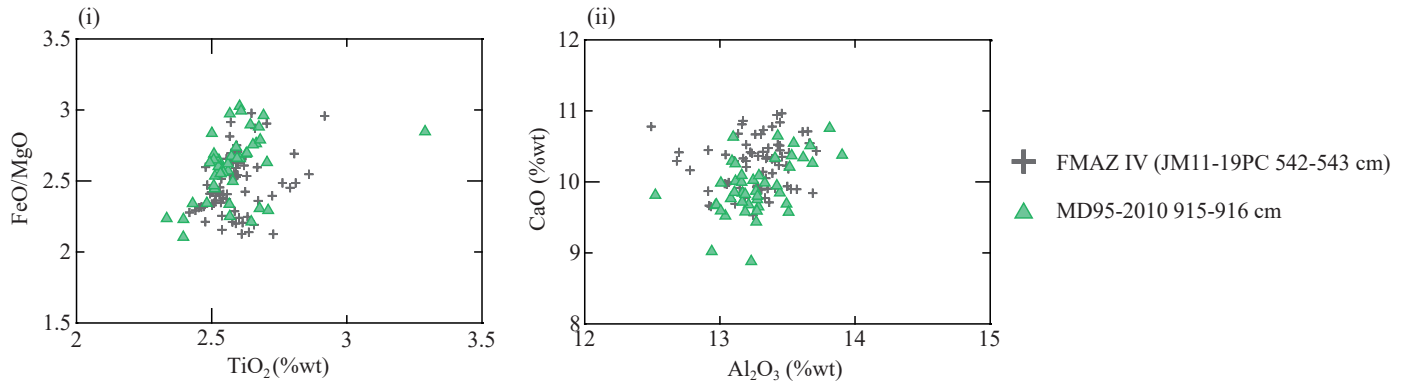
(a) MD99-2251 NAAZ II tephrostratigraphy (Gardar Drift)



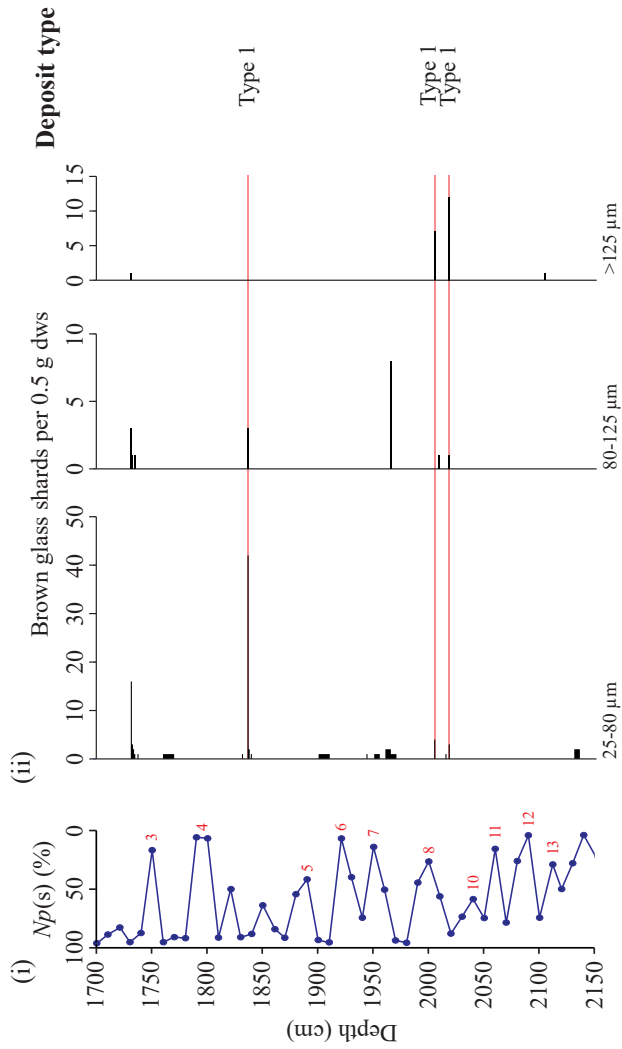
(a) MD95-2010 910-920 cm



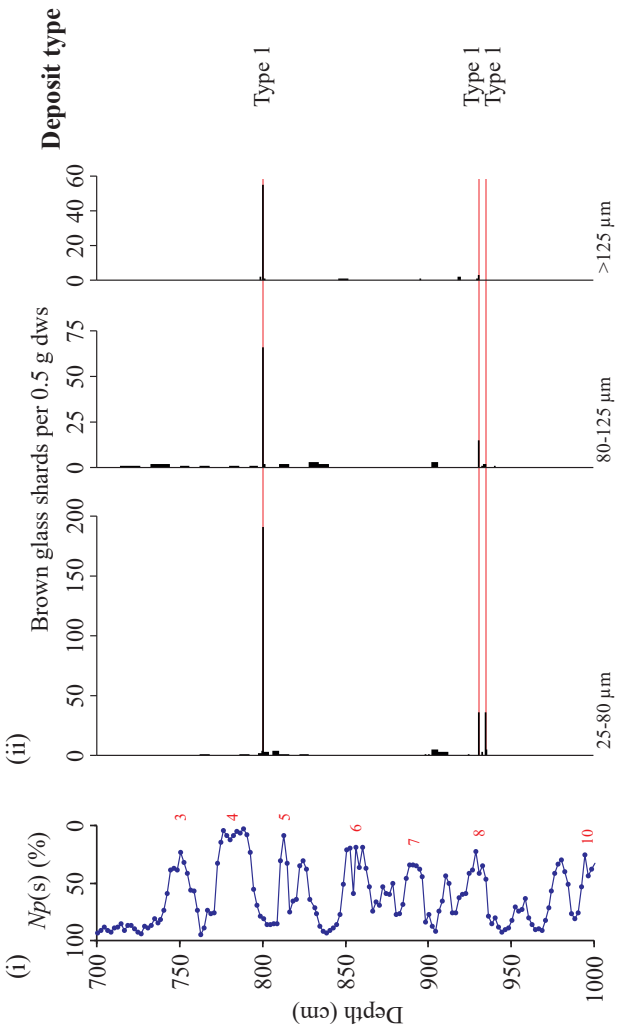
(b)



(a) MD04-2822 (Rockall Trough)



(b) MD04-2829CQ (Rosemary Bank)



(c) MD04-2822 and MD04-2829CQ characterisations

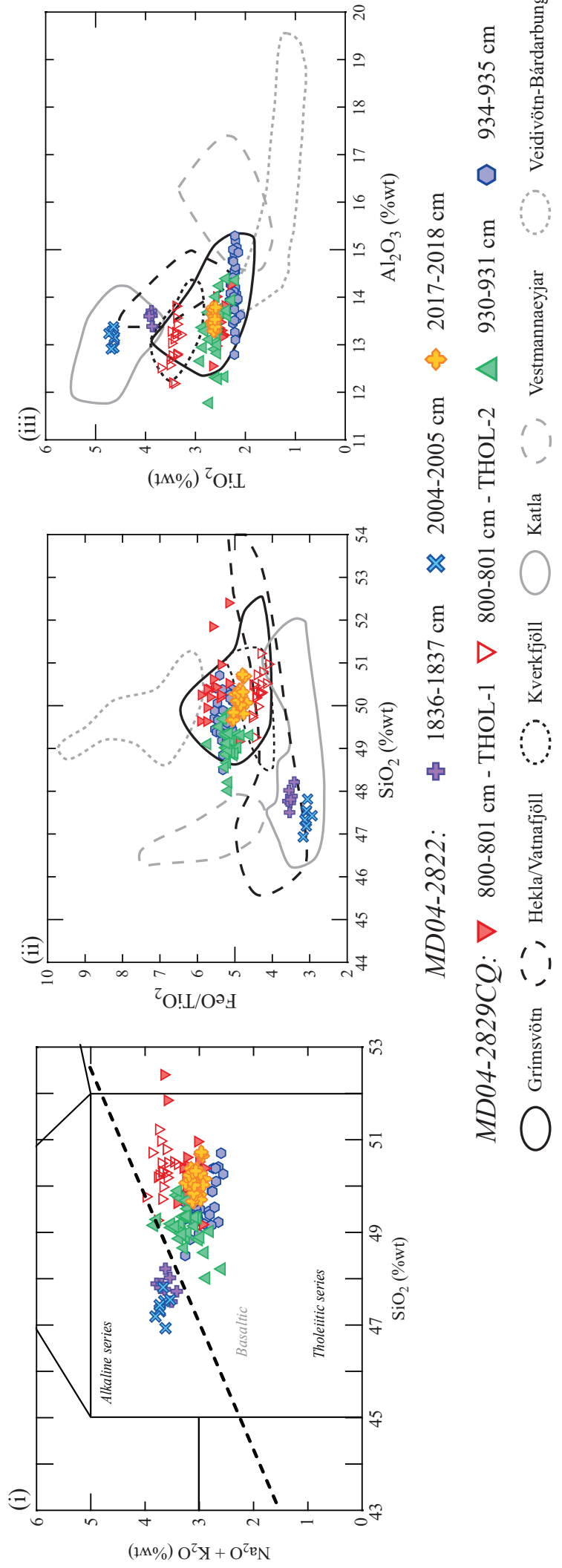
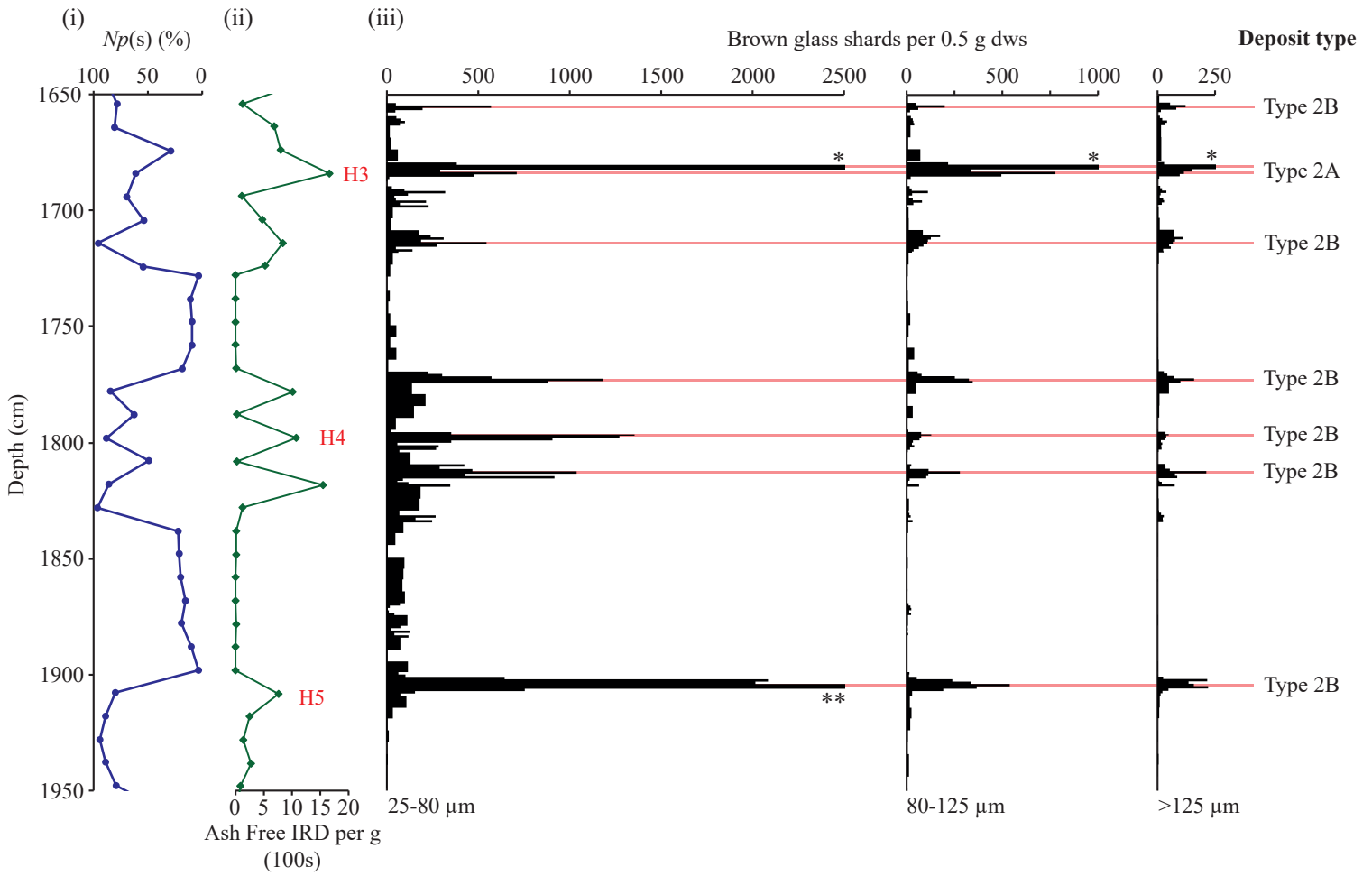
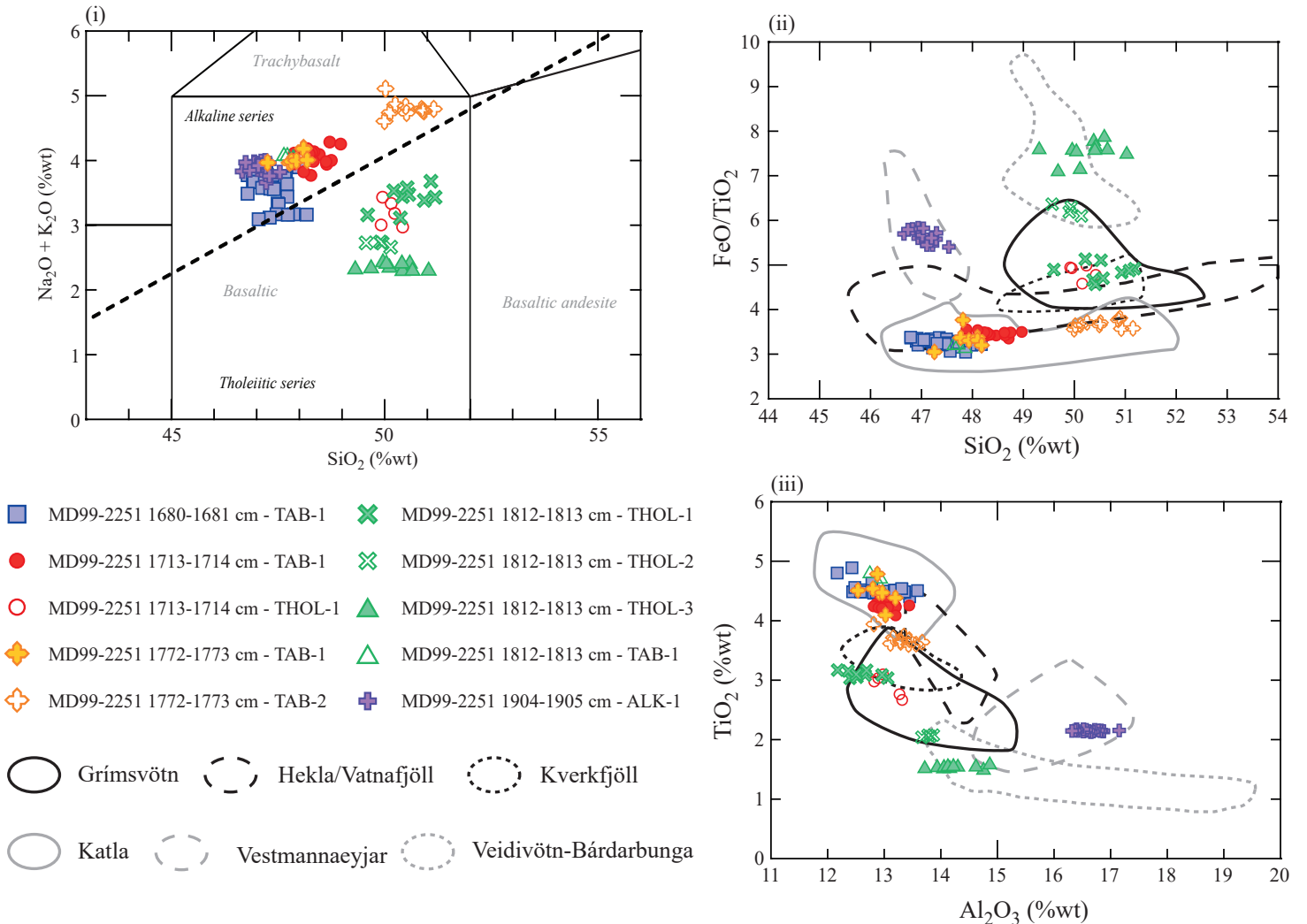


Figure 6

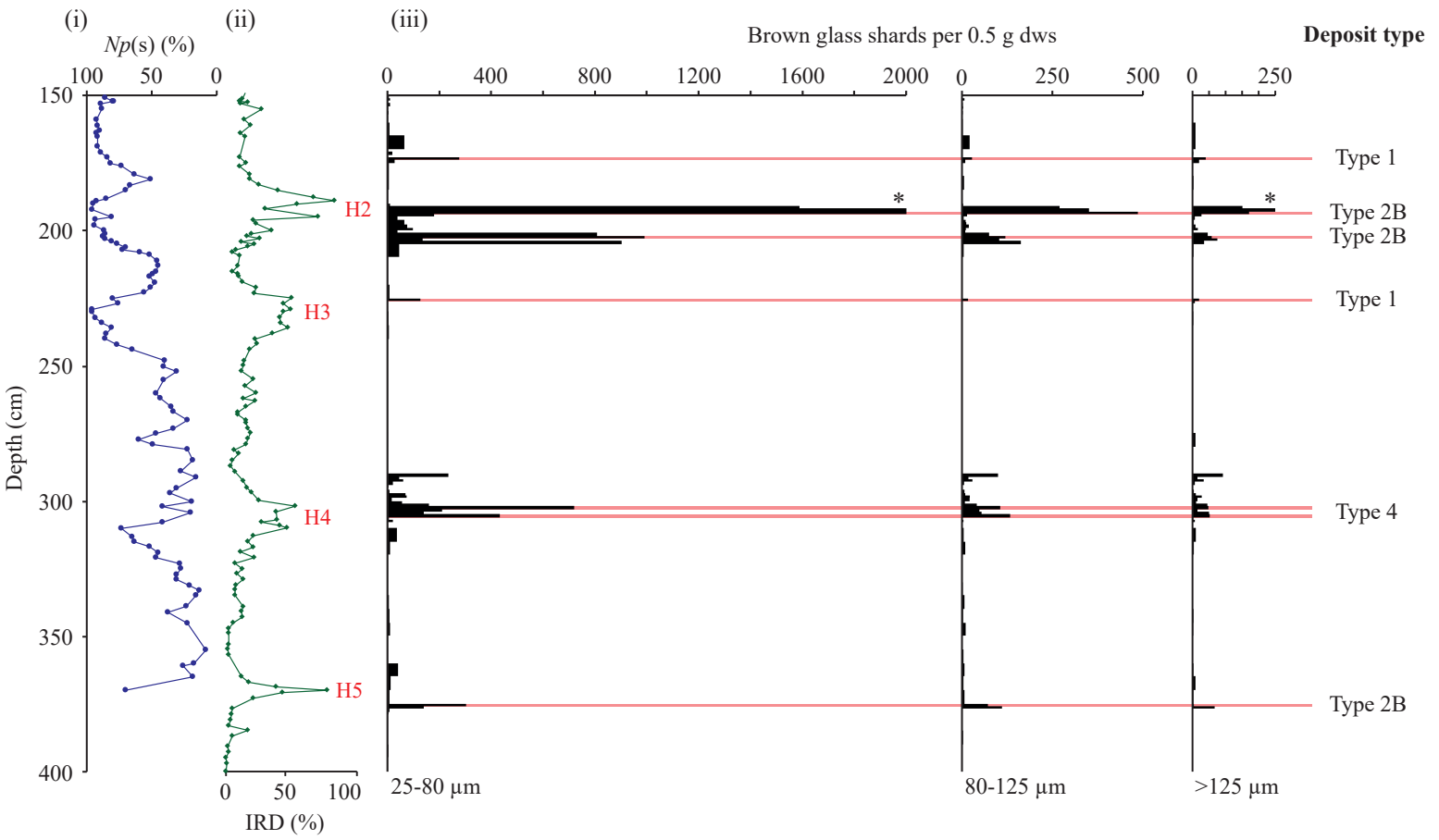
(a) MD99-2251 tephrostratigraphy (Gardar Drift)



(b) MD99-2251 isochronous horizon and significant geochemical populations



(a) GIK23415-9 tepthrostratigraphy (Northern North Atlantic)



(b) GIK23415-9 isochronous horizons and significant geochemical populations

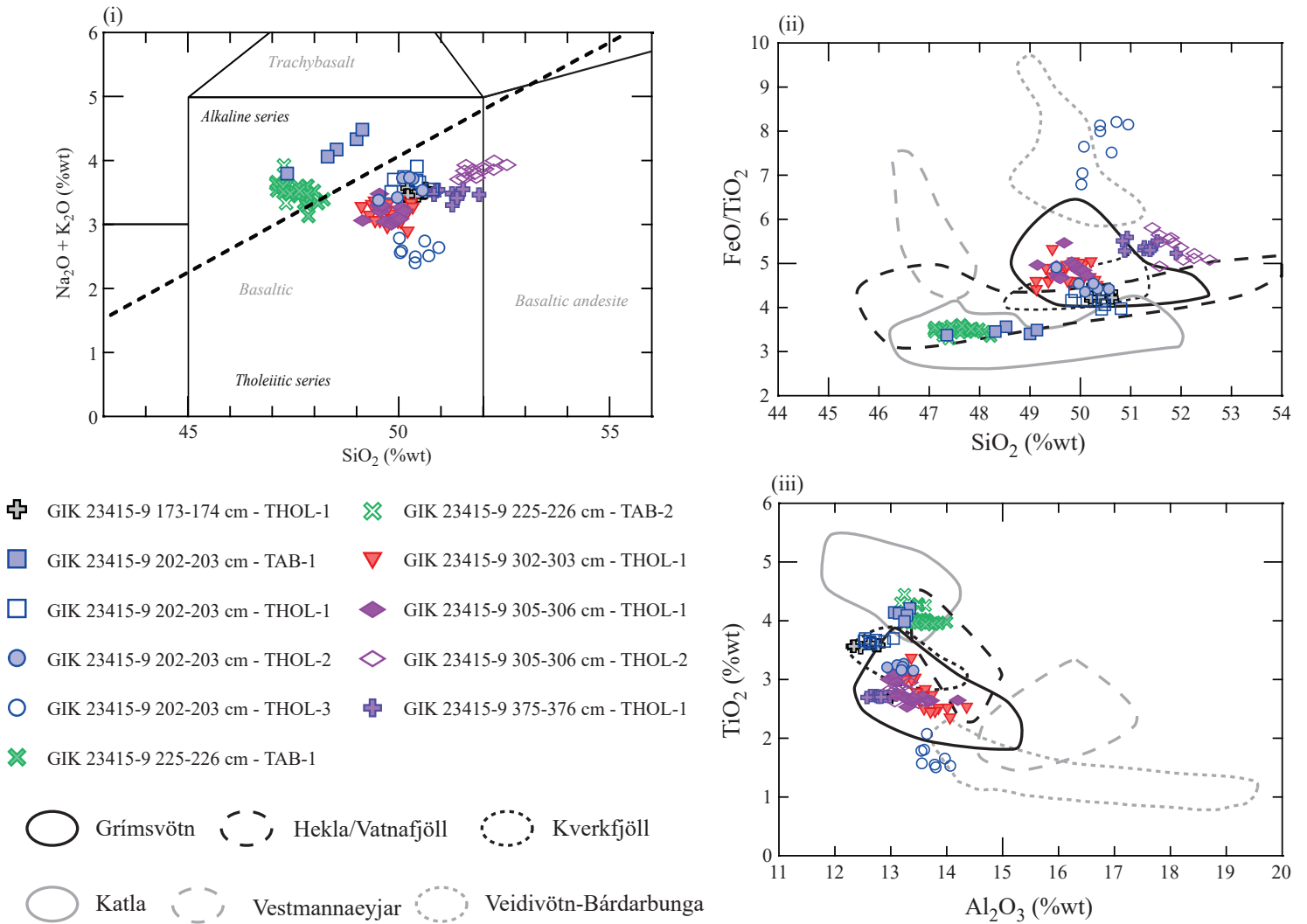


Figure 9

